cxcl18b-defined transitional state-specific nitric oxide drives injury-induced Müller glia cell-cycle re-entry in the zebrafish retina

Aojun Ye[1,3], Shuguang Yu[2], Meng Du[4], Dongming Zhou[4], Jie He[2,*] and Chang Chen[1,3,5,*]

[1]National Laboratory of Biomacromolecules, CAS Center for Excellence in Biomacromolecules, Institute of Biophysics, Chinese Academy of Sciences, Beijing 100101, China

[2]Institute of Neuroscience, State Key Laboratory of Neuroscience, CAS Center for Excellence in Brain Science and Intelligence Technology, Chinese Academy of Sciences, Shanghai 200031, China

[3]University of Chinese Academy of Sciences, Beijing 100049, China

[4]Tianjin Medical University, Tianjin 300070, China

[5]Lead contact

*Correspondence: jiehe@ion.ac.cn, changchen@moon.ibp.ac.cn

Abstract:

In lower vertebrates, retinal Müller glia (MG) exhibit a life-long capacity of cell-cycle re-entry to regenerate neurons following the retinal injury. However, the mechanism driving such injury-induced MG cell-cycle re-entry remains incompletely understood. Combining single-cell transcriptomic analysis and *in-vivo* clonal analysis, we identified previously undescribed *cxcl18b*-defined MG transitional states as essential routes towards MG proliferation following green/red cone (G/R cone) ablation. Inflammation blockage abolished the triggering of these transitional states, which expressed the gene modules shared by cells of the ciliary marginal zone (CMZ), where life-long adult neurogenesis takes place. Functional studies of the redox

properties of these transitional states further demonstrated the regulatory role of nitric oxide (NO) produced by *Nos2b* in injury-induced MG proliferation. Finally, we developed a viral-based strategy to specifically disrupt *nos2b* in *cxcl18b*-defined MG transitional states and revealed the effect of transitional state-specific NO signaling. Our findings elucidate the precision redox mechanism underlying injury-induced MG cell-cycle re-entry, providing insights into species-specific mechanisms for vertebrate retina regeneration.

Key Words: Müller glia, zebrafish retina, cell cycle re-entry, nitric oxide, precision redox, *cxcl18b*.

Introduction:

Unlike mammalian counterparts, retinal Müller glia (MG) in aquatic and amphibian species can enter injury-induced regeneration program**(Goldman, 2014; Lahne et al., 2020b; Wan and Goldman, 2016)**, which unfolds a set of temporal events from glial reactivation, cell-cycle re-entry, new neuron generation, and circuit integration**(Abraham et al., 2024; Powell et al., 2016)**. In zebrafish, MG respond to injury by glial reactivation, which refers to the initial response of quiescent MG, characterized by morphological changes and upregulation of reactive markers (*gfap*, *ascl1a*, *lin28a*) and activation of signaling pathways such as Notch, Jak/Stat, and Wnt (Lahne et al., 2020b; Pollak et al., 2013; Sifuentes et al., 2016; Yao et al., 2016). This is followed by the proliferation phase, in which MG initiate a transcriptional shift toward a progenitor-like state and cell cycle re-entry. Many genes induced by glial reactivation, such as *lin28a*, *sox2*, and *mycb/h*, are required for cell-cycle re-entry and

subsequent neurogenesis **(Gorsuch et al., 2017; Jorstad et al., 2017; Lee et al., 2024; Ramachandran et al., 2010).** Diverse signaling pathways have been identified to participate in this initial regenerative response**(Campbell et al., 2021; Wan and Goldman, 2017).**

In contrast, although forced expression of factors like *Ascl1* or deletion of repressive chromatin regulators can partially reprogram MG into interneuron-like cells in the injured mouse retina**(Hoang et al., 2020; Jorstad et al., 2017)**, the knowledge of the upstream signals that trigger injury-induced cell-cycle re-entry, a critical step for producing neurogenic progenitors, remains limited**(Lenkowski and Raymond, 2014; Vihtelic and Hyde, 2000; Wu et al., 2001)**. The mechanistic understanding of MG cell-cycle re-entry in the injured zebrafish retina will provide critical knowledge for inspiring new strategies for *in-vivo* re-programming MG to repair the human retina.

The intrinsic and environmental factors contribute to injury-induced MG proliferation**(Gao et al., 2021; Lahne et al., 2020b; Xiao et al., 2023)**. Recent efforts in single-cell RNA-sequencing (scRNA-Seq) have identified *ascl1α*, *clcf1*/*crlf1a***(Boyd et al., 2023)**, and *mycb*/*mych***(Lee et al., 2024)** as key intrinsic drivers of injury-induced MG proliferation in the zebrafish retina. Also, the elegant study of MG injury responses across multiple species, including zebrafish, chicken, and mice, revealed the *hmga1/yap1* signaling network as a key regulator of MG reactivation and neurogenesis in the regenerating retina**(Hoang et al., 2020).** Interestingly, previous studies further reported that post-injury MG in the zebrafish is

capable of re-acquiring the regeneration program that largely recapitulates the embryonic retinal developmental program**(Celotto et al., 2023; Hoang et al., 2020; Lahne et al., 2020a; Lyu et al., 2023)**.

In terms of extrinsic cues, two sources, those from damaged neurons and injury-recruited microglia, are considered indispensable for injury-induced MG proliferation**(Leach et al., 2021; White et al., 2017)**. Previous studies have shown that signals derived from various retinal neuron injury models trigger MG regeneration**(Lyu et al., 2023)**. Meanwhile, accumulating evidence increasingly appreciates the role of inflammatory signals derived from injury-recruited microglia, such as *TNFα***(Conner et al., 2014; Nelson et al., 2013)**, cytokines IL-1β, and IL-10**(Lu and Hyde, 2024)**. Notably, inflammatory responses are intrinsically associated with redox signaling, which is involved in the regeneration processes in various non-neuronal tissues**(Breus and Dickmeis, 2021; Jaeschke, 2000; Zhang et al., 2024)**. However, the involvement of the redox signaling resulting from microglia-derived inflammatory signals in MG cell-cycle re-entry following retina damage remains to be clarified. Nitric oxide (NO), a redox signal, has participated in regenerating various tissues in zebrafish, including the heart**(Rochon et al., 2020; Yu et al., 2024)**, spinal cord**(Bradley et al., 2010)**, and fin**(Matrone et al., 2021)**. Endogenous NO is derived from three forms of NO synthase (NOS) in mammals: neuronal NOS (nNOS), endothelial NOS (eNOS), and inducible NOS (iNOS). The zebrafish comprises *Nos1*, a form of neuronal *Nos*, and *Nos2a*/*2b*, two inducible *Nos*.

In this study, we performed single-cell RNA sequencing to characterize the post-

injury MG states in the zebrafish retina following the specific ablation of green/red cone. This comprehensive analysis led us to define a set of previously unknown *cxcl18b*-positive transitional states as an essential route of MG cell-cycle re-entry in response to injury, and the inflammatory was indispensable for the induction of these transitional states. Intriguingly, we found that these *cxcl18b*-defined transitional states exhibited gene patterns shared by cell states in the CMZ, favoring the idea that *cxcl18b*-defined MG transitional states might represent the developmental program conserved by neuronal regeneration beyond embryonic development. A remarkable phenotype of enriched redox features in these gene patterns suggested the importance of redox signaling. The subsequent screening of redox-related genes revealed the essential role of nitric oxide, produced by *Nos2b*, in triggering MG cell-cycle re-entry after the retinal injury. Notably, we developed a sophisticated viral-based approach to achieve the *cxcl18b*-defined MG transitional state-specific knockout of *nos2b* successfully and verified the requirement of transitional state-specific NO signaling in injury-induced MG proliferation. These findings provide novel cellular and molecular insights into this species-specific post-injury MG cell-cycle re-entry process, with potential implications for the development of regenerative medicine strategies.

Results

Single-cell transcriptome analysis reveals the landscape of injury-induced Müller glia states

Zebrafish Müller glia can respond to retina injury by cell cycle re-entry, a critical

step evolutionarily absent from their mammalian counterparts but essential for neuron regeneration**(Goldman, 2014; Powell et al., 2016)**. We created a zebrafish retina injury model by crossing *Tg(opn1lws2: nfsb-mCherry)*^{uom3} (referred to as *Tg(lws2: nfsb-mCherry)*) with *Tg(mpeg1: GFP)* fish, in which the bacterial nitroreductase (NTR) enzyme was specifically expressed in G/R cone. We selectively ablated the G/R cone starting at 5 days post-fertilization (dpf) by a subsequent 120 hours of metronidazole (MTZ) exposure**(Curado et al., 2007; Curado et al., 2008) (Figure 1A and Figure 1-figure supplement 1A)**. G/R cone became significantly reduced in number since 48 hours post-injury (hpi) and was mostly depleted at 120 hpi **(Figure 1B)**. Meanwhile, a number of microglia (marked by *Tg(mpeg1: GFP)*) migrated to the outer nuclear layer (ONL) as early as 48 hpi, peaked at 72 hpi, and began to reduce in number at 96 hpi and onward **(Figure 1C)**. To confirm the identity of these proliferating cells, we performed BLBP immunostaining and observed that the PCNA□ cells were also BLBP□ (**Figure 1–figure supplement 1B**), indicating their MG origin. Notably, in response to G/R cone ablation, the proliferative MG population increased starting at 48 hpi, peaked at 72 hpi, and began to decline since 96 hpi and forward **(Figure 1D)**. Considering the result that the number of proliferative MG peaked at 72 hpi, we focused on the 72-hpi time point for further exploration of MG proliferative behaviors following G/R cone ablation **(Figure 1E)**.

By revisiting previously obtained scRNA-seq data of MG enriched from *Tg(lws2: nfsb-mCherry)* crossed with *Tg(gfap: EGFP)* and *Tg(her4.1: dRFP)* retina before and after G/R cone ablation at 72 hpi**(Krylov et al., 2023)**, we selected 5,932 and 3,999

MG cells and their derived progenies from the uninjured and 72-hpi retina, respectively **(Details in Methods; Figure 1-figure supplement 1C)**. By clustering these cells, we identified 13 clusters, 8 out of which (Clusters 2, 3, 5, 6, 9, 10, 11, and 12) with an increased proportion in response to the G/R cone ablation **(Figure 1-figure supplement 1D)**. Subsequently, we re-clustered cells of these 8 clusters (695 cells of uninjured retinae and 3,477 cells of 72-hpi retinae), aggregating into 10 new clusters. After the quality control procedure, we did not consider Clusters 7/8/9 due to their small populations with ribosomal, dendritic, and doublet features, resulting in 7 clusters for further analysis. (Details in Methods; **Figure 1F)**

We performed the pseudo-time trajectory analysis to reveal the progression of these MG clusters following the cone ablation **(Figure 1G)**. Cluster 4 cells were highly expressing genes related to mature MG (*glula*, *slc1a2b*, *apoeb,* and *rlbp1a*)**(Bernardos and Raymond, 2006; Raymond et al., 2006; Thummel et al., 2008; Yurco and Cameron, 2005)**, the quiescent state (*cx43*)**(Dermietzel et al., 2000; Janssen-Bienhold et al., 1998),** and major MG population marker (*fgf24*)**(Krylov et al., 2023) (Figure 1-figure supplement 1E)**. Furthermore, Cluster 4 began to express *s100α10b* and *gfap*, reactive state makers**(Celotto et al., 2023; Hoang et al., 2020)**, in the injured retinae, but not in the uninjured retina **(Figure 1-figure supplement 1E)**. Thus, we set Cluster 4 as the early transitional MG state.

To examine the transition of these 7 MG clusters, the pseudo-time trajectory showed that the main developmental branch consisted of Clusters 4/1/2 and then became divergent into two sub-branches, including Cluster 0 and 5/3/6 (**Figure 1G)**.

In contrast to the sub-branch of Cluster 0, the sub-branch of Clusters 5/3/6 was highly expressing proliferative cell markers (*pcna, mki67,* and *mcm2*). Within the latter sub-branch, while Cluster 3 and 6 with the highest levels of proliferative cell markers, Cluster 6 began to express neuronal differentiation factors (*otx5, crx,* and *pde6gb*)**(Abalo et al., 2020; Asaoka et al., 2014; Shen and Raymond, 2004) (Figure 1-figure supplement 1E)**. Thus, we identified 6 major post-injury MG states, from the early transitional state (Cluster 4) to three transitional states (Cluster 1/2/5), to finally two proliferative states (Cluster 3/6).

Remarkably, chemokine (C-X-C motif) ligand 18b *(cxcl18b*), an inflammatory chemokine, was uniquely expressed in three transitional states but largely absent from the early transitional Cluster 4 and two proliferative Cluster 3/6. Specifically, while the first *cxcl18b*$^{+}$ transitional state (Cluster 1) was expressing *cx43*, a maker for MG quiescence**(Dermietzel et al., 2000; Janssen-Bienhold et al., 1998)**, the last transitional state (Cluster 5) began to show a weak induction of *ascl1α* **(Ramachandran et al., 2010)**. Immediately following this last transitional state, Cluster 3 started with high *ascl1α* expression and entered the proliferative state with the expression of *pcna* and *mik67* **(Figure 1H)**. Our analysis highlighted a new set of *cxcl18b*-defined MG transitional states preceding *ascl1α* induction, bridging MG from the most original quiescence state to injury-induced proliferation.

Clonal analysis reveals injury-induced MG proliferation via *cxcl18b*-defined transitional states associated with inflammation

To directly verify the presence of *cxcl18b*-defined MG transitional states, we first examined the temporal relationship of *cxcl18b* expression and MG proliferation after the cone ablation using *in situ* hybridization combined with immunostaining of either BLBP (an MG maker) or PCNA (a proliferative cell maker) **(Figure 2A and Figure 2-figure supplement 1A)**. The result showed that as early as 24 hpi, the number of *cxcl18b*$^+$ MG was rapidly peaked with no emergence of proliferative MG **(11 ± 4, n=10 in *cxcl18b*$^+$ MG; mean ± SEM)**, and then *cxcl18b*$^+$ MG continued declining in number over time and reached the lowest level since 96 hpi **(1 ± 1, n=7; mean ± SEM; Figure 2B)**. In contrast, the number of proliferative MG (PCNA$^+$) peaked at 72 hpi and decreased to the lowest level at 120 hpi **(9 ± 2, n=11 in 72-hpi retina; 1 ± 1, n=5 in 120-hpi retina; mean ± SEM; Figure 2B)**. Note that *cxcl18b*$^+$ MG was mostly proliferative at 72 hpi **(Figure 2-figure supplement 1B)**.

To further verify the temporal expression of *cxcl18b* in MG following the cone ablation, we created a new transgenic reporter *Tg(cxcl18b: GFP)* by cloning a 3k-bp-long cis-element of 5'UTR with GFP, allowing real-time monitoring of injury-induced *cxcl18b* expression *in vivo* **(Figure 2C and Figure 2-figure supplement 1C-D)**. Combining this line with PCNA immunostaining, we confirmed the remarkable increase of *cxcl18b* expression (GFP$^+$) at 48 hpi **(0 ± 1, n=4 in uninjured retinas vs 11 ± 4, n=7 in 48-hpi; mean ± SEM; Figure 2D and E)**. Due to the prolonged stay of GFP protein, we could also observe that some GFP$^+$ MG were also PCNA$^+$ **(Figure 2D)**. The result of proliferative MG as a subpopulation of *cxcl18b*$^+$ MG led to an outstanding question as to whether *cxcl18b*-defined MG transitional states represented

an essential route to injury-induced proliferation.

To address it, we created a new transgene *Tg(cxcl18b: Cre-vmhc: mCherry:: ef1α: loxP-DsRed-loxP-EGFP:: lws2: nfsb-mCherry)* to perform the clonal analysis of historical *cxcl18b*-expressing in MG after the G/R cone ablation **(Details in Method; Figure 2-figure supplement 1E)**. After ablating the G/R cone by MTZ treatment at 6 dpf for 3 consecutive days, we found that the number of *cxcl18b* lineage-traced MG (marked by GFP^+) and $PCNA^+$ MG was significantly increased at 72 hpi **(Figure 2F)**. Further analysis showed that all $PCNA^+$ MG were *cxcl18b* lineage-traced MG, indicating the *cxcl18b* lineage-traced MG were the ones who could eventually enter into the cell cycle **(13 ± 2 cells for $PCNA^+$ vs 13 ± 2 cells $PCNA^+$ and GFP^+ MG; percentage of $PCNA^+$ and *cxcl18b*$^+$ vs $PCNA^+$ = 93 ± 2%; n=14; p=0.19; Mean ± SEM; Figure 2G)**. Further analysis showed that at 120 hpi, the time point that the MG proliferation has largely creased, GFP^+ MG with the lineage history of injury-induced *cxcl18b* expression constituted about 44% of GS^+ MG at the central retina, indicating that only about half of MG could enter *cxcl18b*$^+$ transitional states following the cone ablation **(14 ± 3 in GS^+ and GFP^+ MG; 28 ± 4 in GS^+ and GFP^- MG, n=14; $p<0.05$; mean ± SEM; Figure 2I)**. Together, our clonal analysis demonstrated that proliferative MG mostly originated from *cxcl18b*-defined MG transitional states, and 44% central MG could become *cxcl18b* positive. To investigate whether *cxcl18b* was required for MG proliferation following G/R cone ablation, we employed CRISPR-Cas9-mediated gene disruption, using two sgRNAs targeting *cxcl18b* **(Figure 2-figure supplement 1F and G)**. We found that *cxcl18b*

knockout did not reduce MG proliferation after G/R cone ablation at 72 hpi (**13 ± 3, n=11 in WT; 11 ± 3, n=7 in *scramble* sgRNA-injected; 13 ± 3, n=7 in *cxcl18b* sgRNA-injected; mean ± SEM**), suggesting that *cxcl18b* per se does not regulate MG proliferation directly **(Figure 2-figure supplement 1H and I)**. This led us to wonder about the induction of *cxcl18b*-defined MG transitional states.

As an inflammatory chemokine, *cxcl18b* serves as a reliable marker of inflammation and regulates neutrophil recruitment to injury sites**(Goumenaki et al., 2024; Torraca et al., 2017)**. Inflammation has been previously shown to be critical for inducing regenerative responses in adult zebrafish, where it promotes reactive microglia/macrophages and Müller glial proliferation in the retina**(Iribarne and Hyde, 2022; Kyritsis et al., 2012)**. Notably, suppressing the immune response using dexamethasone (Dex) in zebrafish retina reduced microglial reactivation and significantly decreased the number of proliferative MG**(Silva et al., 2020; Zhang et al., 2020)**. In our study, we identified the *cxcl18b*-defined transitional states as the essential routing for MG proliferation after G/R cone ablation. These results prompted us to investigate whether the inflammatory responses mediated by recruited microglia are indispensable for the formation of these *cxcl18b*-defined transitional states.

To address this, we examined *cxcl18b* expression using *Tg(cxcl18b: GFP)* after inhibiting inflammation using Dex**(Iribarne and Hyde, 2022)**, and observed a significant reduction in the number of *cxcl18b*$^+$ MG (GFP$^+$ cells) at 72 hpi **(11 ± 4, n=10 in Dex treated retina vs 19 ± 5, n=6 in DMSO treatment; and 18 ± 3, n=14 in the 72-hpi retina; mean ± SEM) (Figure 2K)**. Consistent with earlier reports, we

observed that Dex treatment inhibited the migration of microglia **(indicated by *Tg(mpeg1: GFP)*; 16 ± 4, n=14 in Dex treated retina vs 27 ± 5, n=7 in DMSO treatment; and 28 ± 4, n=9 in the 72-hpi retina; mean ± SEM)** to the ONL and significantly reduced the number of proliferative MG **(PCNA$^+$; 8 ± 2, n=14 in Dex treated retina vs 17 ± 2, n=7 in DMSO treatment; and 14 ± 3, n=9 in the 72-hpi retina; mean ± SEM)** at 72 hpi after G/R cone ablation **(Figure 2L and M and Figure 2-figure supplement 1J)**. These findings suggest that microglia-mediated inflammation may contribute to the activation of *cxcl18b*-defined transitional states that precede MG proliferation, although a causal relationship remains to be established. While dexamethasone suppressed both microglial recruitment and *cxcl18b*$^+$ MG generation, its broad anti-inflammatory action precludes definitive conclusions about microglial causality. Dissecting this relationship would require concurrent ablation of microglia and cone photoreceptors using a triple-transgenic strategy, which is beyond the scope of the current study. Targeted approaches will be necessary to resolve the specific role of microglia in initiating *cxcl18b* expression.

cxcl18b-defined MG transitional states recapitulate molecular features of retinal stem cells in the ciliary marginal zone

Interestingly, we observed the *cxcl18b* expression in the CMZ after the cone ablation besides its high expression in the MG **(Figure 2A)**. We were then curious about the *cxcl18b* expression in the developmental retina as well as in the CMZ without the injury. Notably, *in situ* results showed that *cxcl18b* was largely absent

from the central region but presented in the peripheral region of 30-hpf retinae, whereas it was highly expressed in the most peripheral region of the CMZ, where *fabp11a* and *col15α1b*, two putative markers for post-embryonic retinal stem cells (RSCs) are located**(Gonzalez-Nunez et al., 2010; Raymond et al., 2006) (Figure 3A-B and E-F, and Figure 3-figure supplement 1A)**. The transgenic line of *Tg(cxcl18b: GFP)* also showed a robust *cxcl18b* expression in the CMZ **(Figure 3-figure supplement 1D)**. Consistently, our scRNAseq data of CMZ cells also confirmed the co-expression of *cxcl18b*, *fabp11a*, and *col15α1b* **(Figure 3C-D and G-H, and Figure 3-figure supplement 1B)**. Furthermore, cluster 1 MG, at the earlier stage of transitional states, has the highest *cxcl18b* expression with *col15α1b* expression **(Figure 1F and Figure 3-figure supplement 1C)**. All these results suggested that *cxcl18b*-defined transitional states, at least to some extent, represent the developmental state of retinal stem cells in the CMZ, but not that of embryonic retinal progenitors.

***Nos2b* is required for MG entry into the proliferation via NO signaling**

Previous studies have demonstrated the involvement of redox signaling in cell regeneration processes in various tissues across species**(Han et al., 2014; Hunter et al., 2018; Matrone et al., 2021; Yoo et al., 2012)**. All these evidences led us to directly test the roles of redox genes in serving as the molecular mechanism underlying injury-induced MG proliferation. Thus, we first examined the expression levels of a comprehensive list of redox genes in *cxcl18b*-defined MG transitional

states (Clusters 1/2/5) in our scRNA-seq data **(Figure 1H)** and screened the influence of 18 genes from each major category of redox signaling on injury-induced MG proliferation using CRISPR-Cas9-mediated gene disruption **(Figure 4-figure supplement 1A)**. We focused on the nitric oxide (NO) signaling pathway, targeting three genes encoding nitric oxide synthases (*Nos*): neuronal *Nos* (*nos1*) and two inducible forms (*nos2a* and *nos2b*), as well as the gene encoding S-nitrosoglutathione reductase (*gsnor* or *adh5*), which modulates reactive NO signaling **(Figure 4A and Figure 4-figure supplement 1B)**. The consequence and efficiency of gene disruption were verified by DNA sequencing **(Figure 4-figure supplement 1C)**. Notably, the disruption of *nos2b* resulted in a significant reduction of $PCNA^+$ MG at 72 hpi **(6±2, n=22 in *nos2b*-disrupted vs 11±3, n=7 in *scramble* sgRNA-injected; Mean ± SEM) (Figure 4B)**. Noted that *nos* gene disruption did not significantly alter microglia recruitment or G/R cone ablation at 72 hpi, suggesting that the influence of NO on injury-induced MG proliferation was not via inflammatory reactions of recruited microglia or injury degree **(Figure 4-figure supplement 1D-F)**.

To further examine the function of *Nos2b* via NO, we employed various *Nos* inhibitors (L-NG-nitro arginine methyl ester, L_NAME; L-NG-Monomethyl Arginine, L_NMMA; 1400W) and NO scavengers (carboxy-PTIO, C-PTIO)**(Goldstein et al., 2003; Hong et al., 2012; Moore et al., 1990; Rees et al., 1990)**. We performed the intraocular injection of the drugs (PBS as control) into the zebrafish eye from 2 days before cell ablation until 72 hpi **(Figure 4C)**. Notably, the NO scavenger C-PTIO mostly suppressed MG proliferation, indicating the involvement of NO **(cell number**

of PCNA^{+} MG: 3±2, n=27 after blocking NO by C-PTIO vs 14±4, n=16 in PBS-injected retina; Mean ± SEM) (Figure 4D and E). Moreover, 1400W (an inhibitor specific to inducible *Nos*, **7±2, n=10; Mean ± SEM**) and L_NAME (a broad inhibitor to all three *Nos* forms, **8±2, n=12; Mean ± SEM**) could also significantly reduce the number of proliferative MG after the ablation, whereas L_NMMA (the inhibitor specific to neuronal *Nos*) did not influence MG proliferation (**11±3, n=12; Mean ± SEM**) **(Figure 4E)**. Taken together, these results highlight the critical role of NO signaling in regulating injury-induced MG proliferation.

We further generated nitric oxide pathway mutant zebrafish (*nos1*, *nos2a*, *nos2b*, and *gsnor*) to investigate the role of NO in MG proliferation following G/R cone ablation. Utilizing CRISPR/Cas9-mediated gene disruption, we successfully screened out *nos1*, *nos2a*, *nos2b*, and *gsnor* mutants, characterized by deletions of 133-bp, 13-bp, 220-bp, and 11-bp coding sequences, respectively (see Methods for details, **Figure 4-figure supplement 2A and B)**. Consistent with the gene disruption experiments described above, we observed a significant reduction in the number of proliferative (PCNA□) MG at 72 hpi following G/R cone ablation in both heterozygous and homozygous *nos2b* mutants (*nos2b*□/□: 3□±□1, *n*□=□20; *nos2b*□/□: 6□±□2, *n*□=□20) compared to WT controls (11□±□2, *n*□=□14; mean□±□SEM). In contrast, no significant changes in MG proliferation were observed in *nos1*, *nos2a*, or *gsnor* mutants compared to wild type **(Figures 4F-4I)**.

Interestingly, the reduction in proliferative MG was more pronounced in *nos2b* heterozygous mutants (*nos2b*$^{+/-}$) than in homozygous mutants (*nos2b*$^{-/-}$) **(*nos2b*$^{+/-}$ vs**

***nos2b*$^{-/-}$; p<0.001; Mean ± SEM) (Figure 4J)**. We observed no significant difference in the loss of cone photoreceptor at 72 hpi between *nos2b* mutants and WT, indicating that the reduced MG proliferation observed in *nos2b* mutants is independent of the injury (WT: 45□±□8 remaining cones, *n*□=□24; *nos2b*□/□: 49□±□12, *n*□=□20; *nos2b*□/□: 46□±□9, *n*□=□20; mean□±□SEM) (Figure 4K). This unexpected result suggests a concentration-dependent effect of NO on proliferative MG. Specifically, compared to homozygous mutants, heterozygous mutants with intermediate NO levels more effectively suppressed MG proliferation, whereas wild-type animals with higher NO levels promoted MG proliferation. This concentration-response pattern highlights the role of NO as a regulator, rather than a mediator, of injury-induced MG proliferation.

Specific *nos2b* expression in *cxcl18b*-defined transitional states MG after G/R cone ablation

To further examine whether the expression of *nos2b* in *cxcl18b*$^{+}$ MG, we used the newly generated transgene fish line in our study *Tg(cxcl18b: GFP)*, enabling us to monitor *cxcl18b*$^{+}$ MG after the G/R cone ablation in a real-time manner. By crossing different fish lines, we fluorescently sorted out three post-injury MG populations (72-hpi MG, 72-hpi PCNA^{+} MG, and 72-hpi *cxcl18b*$^{+}$ MG) and three control groups (uninjured MG, 72-hpi retinal cells other than MG and 72-hpi G/R cone) **(Figure 5A-C)**. The real-time quantitative PCR (RT-qPCR) analysis showed that compared to the three control groups, the expression of *nos2b* was significantly higher in *cxcl18b*$^{+}$ MG

than in 72-hpi MG and 72-hpi PCNA$^+$ MG **(relative expression of *nos2b*: 89±32, repeats n=7 in *cxcl18b*$^+$ MG; 14±17, repeats n=5 in 72-hpi MG; and 1±1, repeats n=6 in PCNA$^+$ MG; Mean ± SEM) (Figure 5D and Figure 5-figure supplement 1D-F)**. Together with the fact that *cxcl18b*$^+$ MG contained PCNA$^+$ and PCNA$^-$ populations in *Tg(cxcl18b: GFP)* **(Figure 2D)**, our result indicated that *nos2b* was specifically expressed in *cxcl18b*$^+$ non-proliferative MG, which agreed with the scRNA-seq result of the specific expression of *cxcl18b* in three transitional states (Clusters 1, 2, and 5; **Figure 1H**). *In situ* hybridization using an HCR molecular probe in the *Tg(lws2: nfsb-mCherry:: cxcl18b: GFP)* fish line also suggests that injury-induced *nos2b* expression was specific in the *cxcl18b*-defined transitional state MG **(Figure 5-figure supplement 1A-C$_3$)**. Thus, our analysis reveals that *nos2b* was specifically expressed in *cxcl18b*$^+$ transitional MG states, particularly in non-proliferative cells.

NO produced by *nos2b* determines *cxcl18b*$^+$ MG entry for proliferation

To further explore the role of *cxcl18b*$^+$ MG-specific *nos2b* in regulating the entry of MG proliferation after the G/R cone ablation, we developed a sophisticated clonal analysis of *cxcl18b*$^+$ MG with genetic disruption of *nos2b* using CRISPR-Cas9 method. To achieve glial type-specific gene manipulation, we employed an adenovirus strain that specifically infects radial glia in zebrafish**(Jia et al., 2019; Liu et al., 2021)**, and confirmed that it could faithfully mark MG in the zebrafish retina **(Figure 6A and B)**. For the clonal analysis, we performed the intraocular injection of

two viruses packaged with elements of *cxcl18b: gal4* and *UAS: Cas9-T2A-Cre-u6: sgRNA (nos2b)* into the eye of *Tg(lws2: nfsb-mCherry:: ef1α: loxP-DsRed-loxP-EGFP)* at 5 dpf, virus packaged with the element of *UAS: Cas9-T2A-Cre-u6: empty* as the control **(Figure 6C-D and Figure 6-figure supplement 1A)**. One day after the virus infection, the fish was treated with MTZ for 3 consecutive days to ablate the G/R cone **(Figure 6E)**.

At 72 hpi, we collected the clones (GFP^+) derived from *cxcl18b* lineage-traced MG and analyzed their proliferative property **(Figure 6F and G)**. The analysis of virus-infected clones (GFP^+) cell cycle re-entry ($PCNA^+$) after G/R cone ablation revealed that only ~23% of GFP^+ MG clones remained $PCNA^+$ in the *nos2b* knockout group, compared to ~75% in the control group **(Figure 6H)**. Note that the efficiency of *nos2b* sgRNAs was confirmed in terms of mutation types and knockout efficiency by sequencing **(Figure 6-figure supplement 1B-D)**.

Taken together, these findings suggested that it is the NO produced by *Nos2b* within *cxcl18b*-defined transitional state MG that specifically drives MG from the transitional state into proliferation following injury, highlighting a pivotal mechanism underlying injury-induced regenerative processes.

NO decreased Notch activity that is responsible for injury-induced MG proliferation

Previous studies have shown that *ascl1α* and Notch signaling are essential for MG proliferation in the injured zebrafish retina**(Conner et al., 2014; Wan et al.,**

2012). Regarding Notch signaling, a high Notch3 expression is reported to maintain MG quiescence. In response to the injury, *notch3* expression is downregulated, but *notch1a* is necessary for the continued proliferation of the progenitors**(Campbell et al., 2022)**. In consistent, we observed that *notch3* and *hey* (the Notch downstream target) were highly expressed in uninjured MG clusters and became reduced from the early transitional state (Cluster4) to the proliferative states **(**Cluster 3 and 6**)**, whereas *notch1a/1b* and *ascl1α* were prominently expressed in the late stage of *cxcl18b*$^{+}$ transitional states (clusters 5) and the proliferative states **(**Cluster 3; **Figure 1H and 7A)**. Interestingly, upstream regulators of Notch signaling activation, such as *fgf8a*, *fgf8b***(Wan and Goldman, 2017)**, and *tgfb3***(Lee et al., 2020)**, were predominantly expressed in clusters 4 and 1, preceding the expression of *cxcl18b* **(Figure 7A)**. These results led us to wonder whether NO regulated *cxcl18b*-defined transitional state MG cell cycle re-entry via the Notch signaling pathway.

To examine the influence of NO signaling blockage on Notch activity dynamics following the cone ablation, we employed a reporter line *Tg(Tp1bglob: EGFP)* (referred to as *Tg(Tp1:EGFP)*), in which EGFP is driven by the TP1 element, the direct target of the intracellular domain of Notch receptors (NICD) that is generated upon Notch activation**(Parsons et al., 2009; Quillien et al., 2014)**. We treated fish with the NO scavenger C-PTIO and MTZ, starting at 5 dpf for 5 continuous days and at 7 dpf for 3 continuous days, respectively, followed by immunostaining for EGFP and PCNA **(Figure 7B)**. Interestingly, *Tp1*: EGFP^{+} MG were significantly reduced at all three injury time points **(cell number of EGFP^{+} clones: 34±3, n=9 in 24-hpi**

retina; 29±3, n=4 in 48-hpi retina; 33±4, n=6 in 72-hpi retina vs 42±1, n=4 in the uninjured retina; Mean ± SEM), demonstrating a decrease in Notch activity following G/R cone ablation **(Figure 7C)**. Notably, this reduction in Notch activation was further rescued by NO blocking using C-PTIO (**cell number of EGFP$^+$ clones: 42±1, n=6 in C-PTIO-treated retina at 24 hpi; 42±2, n=5 at 48 hpi; 44±2, n=7 at 72hpi; Mean ± SEM**), suggesting that NO modulates Notch signaling **(Figure 7C)**. Meanwhile, C-PTIO treatment significantly reduced the number of proliferative MG (marked by PCNA) **(Figure 7D)**. These findings indicated that injury-induced NO suppresses Notch signaling activation, which potentially drives MG to exit quiescence and enter proliferation. Together, our results highlight that NO signaling drove the injury-induced *cxcl18b*-defined transitional state MG to enter proliferation, which may be mediated by Notch pathway regulation.

Discussion:

Our study provides the single-cell transcriptomic landscape of Müller glial state progression following the cone ablation at the larval stage. Combined with clonal analysis, we identified a previously unreported *cxcl18b*-defined transitional MG state as the essential routing for MG cell cycle re-entry. It led to our further genetic analysis, revealing the cell type-specific and concentration-dependent regulatory mechanism of nitric oxide derived from *nos2b* underlying injury-induced MG proliferation. Furthermore, NO signaling accounted for a decreased Notch activity, which has been previously reported to be essential for MG proliferation after the injury. Finally, cell state-specific gene disruption revealed that *cxcl18b*-defined MG transitional state-specific *nos2b* is required for injury-induced MG proliferation, which is a prime example of previously reported "5R" redox regulation(Meng et al., 2021). Thus, our study provides the novel precision redox mechanism underlying MG proliferation in response to cone ablation in the zebrafish retina, opening exciting possibilities for future research and potential therapeutic interventions.

Identification of *cxcl18b*-defined MG transitional states following the cone ablation

Combined scRNA-seq analysis and clonal analysis, we identified a previously unreported transitional MG state, marked by the expression of *cxcl18b*, as the essential routing for MG to re-enter the cell cycle following the retina injury **(Figure 1H, 2F, and 2G)**. To our knowledge, it is the first transitional state verified by *in vivo* clonal analysis to show a faithful prediction of injury-induced MG proliferation. Notably, this *cxcl18b* induction in MG depends on microglial recruitment in response to cone ablation, suggesting this transitional state is an MG response to the signals derived from the inflammatory reaction **(Figure 2K)**. The underlying mechanism of this crosstalk is crucial to be addressed. Interestingly, the *cxcl18b*-containing gene module was also expressed in the CMZ, a region crucial for adult retina neurogenesis for a lifetime **(Figure 3A-D)**. However, its expression is mainly absent from the central regions of the developing retina **(Figure 3F)**. It suggests that the *cxcl18b*-

defined transitional state might represent a developmental state used by constitutive neuron generation programs and injury-induced neuron regeneration programs beyond embryonic development. Furthermore, the *cxcl18b*-defined transitional state exhibits robust redox-related characteristics, such as the expression of *sod1*, *sod2*, and *catalase* **(Figure 4-figure supplement 1A)**. It led to the critical discovery of this study, which showed the essential role of *nos2b* in regulating injury-induced MG proliferation. Unfortunately, our preliminary effects on gene disruption using CRISPR/Cas9 in F0 founders did not observe a significant reduction in the number of proliferative MG after *cxcl18b* disruption **(Figure 2-figure supplement 1I)**. However, a recent study reported the essential role of *cxcl18b* in heart regeneration using mutant fish, providing a mechanism of *cxcl18b* as innate immune signaling in injury-induced tissue regeneration**(Goumenaki et al., 2024)**. Their results raised concern about the efficiency of *cxcl18b* disruption in our system. It is essential to use mutant fish to re-examine the role of *cxcl18b* in injury-induced MG proliferation in the future. Also, we cannot rule out the possibility that other co-factors are involved in the action of *cxcl18b* in MG regeneration, which is another critical issue that needs to be solved in the future.

The possible mechanism of NO signaling underlying injury-induced MG proliferation

Our study, for the first time, demonstrated an essential role of NO signaling in regulating MG proliferation after the cone ablation. However, we still need to understand more about the underlying mechanism. There are two well-characterized molecular events responsible for MG proliferation following the retina injury: a decreased Notch activity and an increased *ascl1α* expression**(Fausett et al., 2008; Jorstad et al., 2017; Ramachandran et al., 2010)**. Previous studies have shown that Notch3 is responsible for this decreased Notch activity, leading to increased Ascl1a through the de-depression mechanism**(Campbell et al., 2021; Sahu et al., 2021).** Interestingly, unlike *notch3*, *notch1a* has been reported to stimulate MG proliferation**(Campbell et al., 2021; Campbell et al., 2022)**. Our scRNA-seq analysis

also showed that as MG progressed into the proliferative states after the cone ablation, *notch3* expression gradually declined **(Figure 7A)**. In contrast, *ascl1α, notch1a, and notch1b* expressions were up-regulated and peaked at the proliferative states **(Figure 7A)**. Thus, both previous studies and our current analysis support the idea that the transcriptional regulation of Notch expression accounts for the decreased Notch activity after the injury. Intriguingly, NO has been reported to activate the Notch1 signaling cascade by promoting the release and accumulation of the Notch1 intracellular domain (NICD) through nitration reactions, subsequently enhancing tumorigenesis and stem-like features in various cellular systems**(Charles et al., 2010; López-Juárez et al., 2017; Villegas et al., 2018)**. It raises the possibility that NO signaling regulates injury-induced MG proliferation through the post-translational modification of Notch3. Previous studies have demonstrated two significant forms of NO-mediated post-modification: S-nitrosylation on cysteines and nitration on tyrosine(Wu et al., 2014). Our preliminary analysis showed that all 11 cysteine residues within the putative γ-secretase-dependent cleavage sites are conserved between Notch1a and Notch3, while notable differences were observed at four tyrosine residues. It leads to an outstanding question of whether NO regulated injury-induced MG proliferation by decreasing Notch activity via tyrosine nitration of Notch3, which is worthwhile to elucidate.

The production of NO signaling in MG following retina damage

Previous studies reported that *cxcl18b* is a reliable inflammatory marker**(Goumenaki et al., 2024; Torraca et al., 2017)** and different inflammation responses modulate MG proliferation in the damaged zebrafish retina**(Iribarne and Hyde, 2022)**. The induction of *cxcl18b* may represent the inflammatory responses of MG after the cone ablation, pointing out the potential link between the inflammatory response and the emergence of NO signaling in MG. Previous studies have demonstrated that iNOS is induced in various tissues by proinflammatory cytokines**(Förstermann and Sessa, 2012; Pacher et al., 2007)**. One of the

approaches to test the role of inflammatory responses is to manipulate the levels of inflammatory responses in MG to see the NO production and MG proliferative behaviors. Also, previous studies appreciate the essential role of electrical activity in tissue regeneration**(Levin, 2009; Qin et al., 2023)**; in particular, calcium signaling has been shown to regulate various molecular pathways for liver regeneration, including the hepatocyte growth factor-Met-tyrosine kinase (HGF-Met) transduction pathway(Bedi et al., 2024) and the epidermal growth factor receptor (EGFR) signaling(Kimura et al., 2023). It is interesting to speculate that the abnormal electrical activity of MG in the injured retina may result in an elevated level of intracellular calcium, which activates calmodulin and induces the conformation change of NOS to NO production**(Hanson et al., 2018; Jones et al., 2007)**. A similar mechanism has been proposed in the long-term potentiation of excitatory post-synaptic structure**(Grover and Teyler, 1990; Kawamoto et al., 2012; Park, 2018)** as well as in the glutamate neurotoxicity model**(Ashpole et al., 2013; Ashpole et al., 2012)**. Thus, the production of NO derived from *Nos* may be the product of the interplay between the inflammatory responses and the electrical activity in MG after the retina damage.

Limitations of this study

A few limitations of this study should be acknowledged: 1. Our study focuses on larval zebrafish, in which the core features of MG and immune responses are conserved compared to the adult. However, we acknowledge that the adult retina—with its fully matured differentiated retina and immune response — provides irreplaceable biological insight. Nevertheless, larval models offer a powerful platform to uncover conserved regenerative mechanisms and serve as a valuable complement for identifying age-dependent differences in MG-mediated regeneration. 2. While our data suggest that injury-induced NO suppresses Notch signaling activation and promotes MG proliferation, the use of a general NO scavenger (C-PTIO) does not allow us to determine whether this regulation occurs in an autocrine or paracrine manner. The specific role of NO signaling within *cxcl18b*□ MG requires further

validation using MG-specific NO depletion. 3. The current study's description of the landscape of MG transitional states is based on single-cell transcriptomic data obtained at a single time point (72 hpi) after the cone ablation, which may not provide a complete picture of the state transition of post-injury MG. Future scRNA-seq analysis of MG at multiple post-injury time points is necessary to clarify this issue. 4. While we demonstrated a critical role of NO in injury-induced MG proliferation, the potential contribution of microglia-derived NO was not directly examined. 5. We did not perform direct measurements of NO levels specifically within *cxcl18b*-defined MG cells, leaving open the question of localized NO signaling.

Acknowledgments

This research was supported by grants from the National Key R&D Program of China (2022YFA1303000 to C.C.), the Chinese Academy of Sciences Strategic Priority Research Program B grants (XDB39000000 to C.C.), National Natural Science Foundation of China-Key program project (Grant No. 91849203 to C.C.), the Creative Research Groups of the National Natural Science Foundation of China (32321003 to J.H.), STI2030-Major Projects (2021ZD0204500 to J.H.), the National Key Research and Development Program of China (2020YFA0112700 to J.H.), National Natural Science Foundation of China (32471029 to J.H.).

Author Contributions

A.Y., design and experimental investigation, visualization, data analysis, methodology, writing-original draft, writing-review and editing. S.Y., M.D., and D.Z., investigation, methodology. J.H. and C.C., conceptualization, experimental design, data analysis, supervision, funding acquisition, writing-original draft, project administration, writing-review and editing.

Declaration of Interests

The authors declare no competing interests.

STAR METHODS

Detailed methods are provided in this version of this paper and include the following:

KEY RESOURCES TABLE
RESOURCE AVAILABILITY
Lead contact
Materials availability
Data and code availability
EXPERIMENTAL MODEL AND SUBJECT DETAILS
Single-cell RNA sequencing data analysis
Pseudo-time trajectory analysis
Zebrafish husbandry and transgenic fish lines
Generation of *Tg(cxcl18b: GFP)*
Generation of *Tg(cxcl18b: Cre-vmhc: mCherry:: ef1α: loxP-DsRed-loxP-EGFP:: lws2: nfsb-mCherry)*
Generation of mutant fish lines
Plasmid construction
Clone analysis of *cxcl18b* lineage-traced MG
Metronidazole treatment
Gene disruption via CRISPR/Cas9 system
Pharmacological Treatment with NO scavenger and dexamethasone or *Nos* Inhibitors intraocular injection
The real-time quantitative PCR after FACS-sorted MG
Construction and injection of adenoviral-based MG-specific knockout system in the zebrafish retina
Tissue preparation and immunostaining
In situ hybridization
Imaging
Quantifications and statistical analysis

Key Resources Table

Key Resources Table				
Reagent type (species) or resource	**Designation**	**Source or reference**	**Identifiers**	**Additional information**
strain, strain background (Danio rerio)	Wild type	Dr William		AB
strain, strain background (Danio rerio)	*lws2: nfsb-mCherry*	(Krylov et al., 2023)		*Tg(opn1lws2: nfsb-mCherry)^{uom3}*
strain, strain background (Danio rerio)	*her4.1: dRFP*	(Yeo et al., 2007)	ZDB-TGCONSTRCT-070612–2	*Tg(her4.1: dRFP)*
strain, strain background (Danio rerio)	*gfap: EGFP*	(Bernardos and Raymond, 2006)	ZDB-FISH-150901–29307	*Tg(gfap: EGFP)*
strain, strain background (Danio rerio)	*mpeg1: GFP*	(Ellett et al., 2011)	ZDB-TGCONSTRCT-170801–5	*Tg(mpeg1: GFP)*
strain, strain background (Danio rerio)	*Tp1bglob: EGFP*	(Yu and He, 2019)		*Tg(Tp1bglob: EGFP)*
strain, strain background (Danio rerio)	*pcna: GFP*	(Xu et al., 2020)	ZDB-LAB-070129-2	*Tg(pcna: GFP)*
strain, strain background (Danio rerio)	*ef1α: loxP-DsRed-loxP-EGFP*	(Hans et al., 2009)		*Tg(ef1α: loxP-DsRed-loxP-EGFP)^{zf284}*
strain, strain background (Danio rerio)	*cxcl18b: Cre-vmhc: ECFP*	This manuscript		*Tg(cxcl18b: Cre-vmhc: ECFP; ef1α: loxP-DsRed-loxP-EGFP; lws2: nfsb-mCherry)*
strain, strain background (Danio rerio)	*cxcl18b: GFP*	This manuscript		*Tg(cxcl18b: GFP)*

antibody	Mouse monoclonal anti-PCNA	Abcam	Cat#Ab29; RRID: AB_303394	IF(1:500)
antibody	Rabbit polyclonal anti-BLBP	Abcam	Cat#ab32423; RRID: AB_880078	IF(1:1000)
antibody	Mouse monoclonal anti-Glutamine Synthetase	BD Biosciences	Cat# 610518; RRID: AB_397880	IF(1:1000)
antibody	Chicken monoclonal anti-GFP	Abcam	Cat# ab13970; RRID: AB_300798	IF(1:2000)
antibody	Rabbit polyclonal anti-GFPtag	Rabbit polyclonal anti-GFPtag	Cat#50430–2-AP; RRID: AB_11042881	IF(1:500)
antibody	Rabbit polyclonal anti-DsRed2	Takara Bio	Cat#632496; RRID: AB_10013483	IF(1:1000)
antibody	Alexa Fluor 488 AffiniPure Goat Anti-Mouse IgG (H+L)	Yeasen Biotech	Cat# 33206ES; RRID: AB_3662603	IF(1:1000)
antibody	Alexa Fluor 488 AffiniPure Donkey Anti-Rabbit IgG (H+L)	Yeasen Biotech	Cat# 34206ES60; RRID: AB_2909605	IF(1:1000)
antibody	Alexa Fluor 488 AffiniPure Donkey Anti-Chicken IgY (IgG) (H+L)	Jackson ImmunoResearch Labs	Cat# 703-545-155; RRID: AB_2340375	IF(1:1000)
antibody	Alexa Fluor 594 AffiniPure Donkey Anti-Mouse IgG (H+L)	Yeasen Biotech	Cat# 34112ES; RRID: AB_3661960	IF(1:1000)

antibody	Alexa Fluor 594 AffiniPure™ Goat Anti-Rabbit IgG (H+L)	Yeasen Biotech	Cat# 33112ES; RRID: AB_3661961	IF(1:1000)
antibody	Alexa Fluor 647-AffiniPure Goat Anti-Mouse IgG + IgM (H+L)	Jackson ImmunoResearch Labs	Cat# 115-605-044; RRID: AB_2338906	IF(1:1000)
recombinant DNA reagent	pTol2-cxcl18b: GFP	This manuscript		We made this plasmid by ligated the cxcl18b promoter and GFP element
recombinant DNA reagent	pTol2-cxcl18b: Cre-vmhc: mcherry	This manuscript		We made this plasmid by ligated the cxcl18b promoter and Cre element
recombinant DNA reagent	pTol2-cxcl18b: gal4FF	This manuscript		We made this plasmid by ligated the cxcl18b promoter and gal4FF element
recombinant DNA reagent	pUAS: Cas9T2ACre; U6: sgRNA1; U6: sgRNA2	(Di Donato et al., 2016)	Addgene plasmid #74010; RRID: Addgene_74010	
recombinant DNA reagent	pTol2-UAS: Cas9-T2A-Cre-U6: nos2b sgRNA1; U6: nos2b sgRNA2	This manuscript		We made this plasmid by insert two sgRNAs of *nos2b* in 10xUAS backbone
commercial assay or kit	MEGAscriptTM T7 High Yield Transcription Kit	Invitrogen	Cat# AM1334	
commercial assay or kit	ClonExpress MultiS One Step Cloning Kit	Vazyme	Cat# C113-02	

commercial assay or kit	DIG RNA labeling kit	Roche	Cat# 11277073910	
chemical compound, drug	N(ω)-nitro-L-arginine methyl ester	Sigma-Aldrich	Cat# N5751-1G	10 mM
chemical compound, drug	N(ω)-Methyl-L-arginine acetate salt	Sigma-Aldrich	Cat# M7033-5MG	10 mM
chemical compound, drug	1400W dihydrochloride	MedChemExpress	Cat# HY-18730	200 nM
chemical compound, drug	Phenyl-4,4,5,5-tetramethyl imidazoline-1-oxyl 3-oxide	Sigma-Aldrich	Cat# P5084-25MG	10 mM
chemical compound, drug	Dexamethasone	Sigma-Aldrich	Cat# D1756	10 mM
chemical compound, drug	Metronidazole	Sigma-Aldrich	Cat# M3761-100G	10 mM
software, algorithm	FV10-ASW 4.0 Viewer	Olympus	www.olympus-global.com	Analysis image
software, algorithm	GraphPad Prism V 9.0.0	GraphPad Software	www.graphpad.com	Data analysis
software, algorithm	Cell Ranger Single Cell Software Suite (v2.1.0)	10x genomics	https://support.10xgenomics.com	scRNA-seq data analysis
software, algorithm	RStudio	RStudio IDE	https://posit.co/	scRNA-seq data analysis
software, algorithm	R 4.4.1	R-project	https://www.r-project.org/	scRNA-seq data analysis

software, algorithm	Seurat	Satijalab	https://satijalab.org/seurat/	scRNA-seq data analysis

Resource availability

Lead contact

Further information and requests for resources and reagents should be directed to and will be fulfilled by the lead contact, Chang Chen (changchen@moon.ibp.ac.cn).

Materials availability

All unique reagents generated in this study will be made available from the contact. We may require a completed MTA if there is potential for commercial application.

Data and code availability

This paper does not report new raw scRNA-seq data and original code.
Any additional information required to reanalyze the data reported in this paper is available from the lead contact upon request.

Experimental Model and Subject Details

Single-cell RNA sequencing data analysis

In this study, single-cell RNA sequencing (scRNA-seq) raw data of Müller glia enriched after G/R cone ablation at 72 hpi are from**(Krylov et al., 2023)**, embryonic RPCs at 24 hpf, and postembryonic retinal stem cells (RSCs) at 14 dpf are from**(Xu et al., 2020)**. We re-processed the single-cell FASTQ sequencing reads (Novogene) and converted to digital gene expression matrices using the Cell Ranger software (version 3.1.0) provided by 10X Genomics after mapping to the zebrafish GRCz11 (Ensembl release-96) genome assembly. An average of 47,545 mean reads per cell with 1,343 median genes per cell in no ablation control, 63,177 mean reads per cell with 1,556 median genes per cell in G/R cone ablation (lws2_72 hpi), 61,772 mean reads per cell with 2,474 median genes per cell in the embryonic RPCs at 24 hpf, and 49,243 mean reads per cell with 1,181 median genes per cell in the postembryonic retinal stem cells (RSCs) at 14 dpf were obtained.

We then used the *cellranger aggr* (version 6.0, https://support.10xgenomics.com/single-cell-gene-expression/software/pipelines/latest/using/aggregate) to aggregate the *cellranger* counts from the two datasets and normalize them to the same sequencing depth. The feature barcode matrix was recalculated and analyzed on the combined data. This resulted in a dataset of 19,706 aggregated cells, with 100% of the no ablation control reads retained and 71.4% of the *lws2_3 dpi* reads retained. The aggregated matrix for the no ablation control and lws2_72 hpi samples was loaded into the Seurat R package (version 4.3.0, https://satijalab.org/seurat/). Cells with gene expression of more than 200 and less than 4000, lower than 5% mitochondrial content were filtered for further analysis. The filtered data were normalized, scaled, and clustered using principal component analysis (PCA) with a significance threshold of $p < 0.001$ (FindClusters, resolution = 0.5), and a UMAP was computed using scanpy.tl. umap, resulting in 20 distinct clusters. MG clusters were identified by high expression of marker genes, including *rlbp1a*, *fabp7a*, *slc1a2b*, *glula*, *glulb*, *gfap*, and *her4.1*. Proliferative MG clusters were identified from proliferative cell clusters by high expression of

proliferative cell markers, including *pcna*, *mki67*, *gfap*, *her4.1*, and low expression of the CMZ markers, including *fabp11a*, *col15α1b*, *fabp7b*, *rx2*. We further analyzed the MG and proliferative MG clusters to obtain 13 clusters, including no ablation control 5,932 cells and G/R cone ablation 72 hpi 3,999 cells in the UMAP plot **(Figure 1-figure supplement 1C)**. We compared the proportion of cell numbers in each cluster before and after injury and chose clusters with a high proportion of cell numbers in G/R cone ablation 72 hpi (clusters 2, 3, 5, 6, 9, 10, 11, 12, and 13) to further cluster into 10 clusters **(Figure 1-figure supplement 1D)**.

Single-cell RNA sequencing data of embryonic RPCs at 24 hpf and postembryonic RCSs at 14 dpf were generated into 10 and 11 clusters, respectively. Each cluster is identified by the cluster-specific marker gene and different development stage markers, including *fabp11a*, *col15α1b*, *cxcl18b*, *her4.2*, *npm1a*, *her9*, *fabp7a*, *dla*, *atoh7*, *vsx1*, *mafba*, *otx5*, and *rem1* (**Figure 3A, 3C and Figure 3-figure supplement 1A and B**).

Pseudo-time trajectory analysis

After the UMAP cluster analysis of the single-cell data, trajectory analysis was performed to investigate the pseudo-time transcriptomic change of these ten clusters using the 'monocle 2' R package, which revealed three distinct states **(Figure 1G)**.

Zebrafish husbandry and transgenic fish lines

All experimental zebrafish embryos, larvae, and adults were produced, grown, and maintained at 28°C according to standard protocols. Embryos and larvae were kept in embryo medium (E3; 5 mM NaCl, 0.17 mM KCl, 0.33 mM $CaCl_2 \cdot 2H_2O$, 0.33 mM $MgSO_4 \bullet 7\ H_2O$, 1.3×10^{-5} % w/v methylene blue in RO water) at 28.5 °C, under a 14:10 light: dark cycle. Animal procedures performed in this study were approved by the Animal Use Committee of the Institute of Neuroscience, Chinese Academy of Sciences (NA-069-2023).

Published fish lines used in this study include the following: AB (Wild type, WT) and transgenic lines (Tg): *Tg(opn1lw2: NTR-mCherry)*^{uom3} (ZDB-ALT-201012-

2)**(Wang et al., 2020)** in this study named *Tg(lws2: nfsb-mCherry)*, *Tg(gfap: EGFP)*^{mi2001} (ZDB-FISH-150901–29307)**(Bernardos and Raymond, 2006)**, *Tg(her4.1: dRFP)* (ZDB-TGCONSTRCT-070612–2)**(Yeo et al., 2007)**, *Tg(mpeg1: GFP)* (ZDB-TGCONSTRCT-170801–5)**(Ellett et al., 2011)**, *Tg(pcna: GFP)* (ZDB-LAB-070129-2)**(Xu et al., 2020)**, *Tg(ef1α: loxP-DsRed-loxP-EGFP)***(Hans et al., 2009)**, *Tg(Tp1bglob: EGFP)***(Yu and He, 2019)**.

Newly generated transgenic fishline contained: *Tg(cxcl18b: GFP)*, *Tg(cxcl18b: Cre-vmhc: mCherry:: ef1α: loxP-DsRed-loxP-EGFP:: lws2: nfsb-mCherry)*, and mutants *nos1*$^{+/-}$, *nos2a*$^{+/-}$, *nos2b*$^{+/-}$, *gsnor*$^{+/-}$, *nos1*$^{-/-}$, *nos2a*$^{-/-}$, *nos2b*$^{-/-}$, *gsnor*$^{-/-}$.

Generation of *Tg(cxcl18b: GFP)*

The plasmid of *pTol2-cxcl18b: GFP* (10 ng/ μl) and *tol2* mRNA (50 ng/ μl) were co-injected into a wild-type embryo at the one-cell stage. Zebrafish embryos with green fluorescent were grown at the E3 medium according to standard protocol and selected as the founder (F0). The adult F0 fish crossed with the wild-type selected the fish with GFP^{+} offspring as F1. In this stable transgenic line, *cxcl18b*$^{+}$ cells expressed the fluorescent protein GFP and the full name of this line is *Tg(cxcl18b: GFP)*.

Generation of *Tg(cxcl18b: Cre-vmhc: mCherry:: ef1α: loxP-DsRed-loxP-EGFP:: lws2: nfsb-mCherry)*

The plasmid of *pTol2-cxcl18b: Cre-vmhc: mCherry* (10 ng/ μl) and *tol2* mRNA (50 ng/ μl) were co-injected into the embryo obtained from *Tg(lws2: nfsb-mCherry)* cross *Tg(ef1α: loxP-DsRed-loxP-EGFP)* at the one-cell stage. Zebrafish embryos were maintained at E3 medium according to standard protocol. Larvae with *mCherry* expression in the heart and eyes were selected and grown as the founder (F0) for further construction. The adult founder was crossed with wild-type (AB), considering the expression of *cxcl18b* during zebrafish development, larvae with mCherry and GFP double positive were selected and grown as the F1. In this zebrafish line, EGFP permanently marks all cells that have expressed *cxcl18b*, as well as their entire lineage of progeny. The full name of this line is *Tg(cxcl18b: Cre-vmhc: mCherry:: ef1α: loxP-DsRed-loxP-EGFP:: lws2: nfsb-mCherry)*.

Generation of mutant fish lines

The CRISPR/Cas9 system was employed to efficiently and precisely generate mutant zebrafish lines**(Wu et al., 2018)**. Two sgRNAs targeting gene coding sequences involved in nitric oxide metabolism signaling (nitric oxide synthase, *Nos*; and S-nitrosoglutathione reductase, GSNOR) were designed based on the zebrafish GRCz11 genome assembly.

Primers were designed approximately 200 bp from the sgRNA target sites for genotyping (sgRNAs and genotyping primers are listed in **Supplementary Table S1**). We mixed the two sgRNAs (100 ng/μl) for each target gene with Cas9 protein (400 ng/μl) and injected them into transgenic fishline *Tg(lws2: nfsb-mCherry)* embryos at the one-cell stage. Adult fish were crossed with wild-type, and offspring displaying *mCherry* expression in the eyes at 5 dpf were selected for further genotyping. Mutants were confirmed by sequencing, and the fish with open reading frame (ORF) shift were collected as heterozygous fish for further studies.

Plasmid construction

We cloned the *cxcl18b* regulatory element (3048 bp upstream of the start codon including the *5'UTR*) as the *cxcl18b* promoter from the zebrafish genomic DNA **(Figure 2C)**. The primers used for amplification were 5'-GCATTTGTCTCCTCATGCATTGACTAC-3' (forward primer) and 5'-TTGCTGCAAACTATATGTAGGAAATGCTG-3' (reversed primer). For constructing the plasmids *pTol2-cxcl18b: GFP*, *pTol2-cxcl18b: Cre-vmhc: mCherry*, and *pTol2-cxcl18b: gal4FF*, each DNA elements cassette was inserted into the *pDestTol2pA2* vector**(Kwan et al., 2007)**. The plasmid of *pUAS: Cas9T2AGFP; U6: sgRNA1; U6: sgRNA2* was kindly provided by Professor Filippo Del Bene.**(Di Donato et al., 2016)**. To prepare for plasmid *pTol2-UAS: Cas9-T2A-Cre-U6-empty* and *pTol2-UAS: Cas9-T2A-Cre-U6: nos2b sgRNA1; U6: nos2b sgRNA2*, the same two *nos2b* sgRNAs used to construct *nos2b* mutant fish were inserted into *pUAS: Cas9T2AGFP; U6: sgRNA1; U6: sgRNA2* plasmid, with the *GFP* element replaced by *Cre* using

ClonExpressMultiS One Step Cloning Kit (Vazyme, C113□02). For the plasmid construction of the MG-specific knockout system based on recombinant adenoviral vectors, regulatory elements were inserted into adenoviral vectors *pAdc68-S* according to the standard protocol outlined by Jia et al.**(Jia et al., 2019)**. The final plasmids generated included, *pAdC68XY2-E1-CMV-GFP pAdC68XY2-E1-10xUAS: Cas9-2a-Cre-U6: sgRNA1(nos2b); U6: sgRNA2(nos2b), pAdC68XY2-E1-cxcl18b: gal4FF* and *pAdC68XY2-E1-10xUAS: Cas9-2a-Cre-U6: empty* as the control. Plasmid construction primer sequences are listed in **Supplementary Table S2**.

Metronidazole treatment

Zebrafish larvae were exposed to a 10 mM metronidazole (MTZ) solution (Sigma-Aldrich, M3761-100G) in standard fish water. For *Tg(lws2: nfsb-mCherry)* larvae processed for immunohistochemical analysis, MTZ treatment was initiated at 6 dpf to ablate green and red cones. Larvae were maintained in the MTZ solution at densities of fewer than 50 larvae per 50 mL petri dish and kept at 28.5°C. The MTZ solution was refreshed every 24 hours to ensure continuous cone ablation until fixation in 4% PFA, while control larvae were kept in standard fish water.

Clone analysis of *cxcl18b* lineage-traced MG

Clone analysis of *cxcl18b*$^{+}$ lineage-traced MG was restricted to cells located in the central and dorsal region of the zebrafish retina after G/R cone ablation in Figure 2, Figure 6, and their figure supplement. This spatial restriction strongly suggests that the proliferative MG originate from local mature MG, although we cannot completely rule out the possibility that CMZ-derived progenitors contribute to the generation of proliferative MG in the peripheral retina.

Gene disruption via CRISPR/Cas9 system

We used the CRISPR/Cas9 system for efficient gene disruption. Two sgRNAs were designed to target the coding sequences of genes involved in the nitric oxide signaling pathway (including *nos1*, *nos2a*, *nos2b*, *gsnor*) and *cxcl18b*. The sgRNAs

were in vitro transcribed and purified using the LiCl precipitation approach (MEGAscript T7 Transcription Kit, Invitrogen, AM1334). A mixture of the two sgRNAs (in total 200 ng/μl) with Cas9 protein (400 ng/μl, Novoprotein, E365 01A) were co-injected into the embryo of *Tg(lws2: nfsb-mCherry)* at the one-cell stage. The efficiency of gene knockout for each sgRNA was validated, as presented in **Figure 4-figure supplement 1C**.

Pharmacological treatment with NO scavenger and dexamethasone or *Nos* Inhibitors intraocular injection

Zebrafish larvae at 6 dpf were anesthetized in 0.04% MS222 (Sigma, A5040) for 30 to 45 seconds. Inhibitor solutions of 2 μL were prepared as follows: 10 mM *N(ω)*-nitro-L-arginine methyl ester (L-NAME, Sigma-Aldrich, N5751-1G), a broad *Nos* inhibitor, diluted in sterile PBS from a 100 mM stock; 10 mM N(ω)-Methyl-L-arginine acetate salt (L-NMMA, Sigma-Aldrich, M7033-5MG), a specific inhibitor of *nNos*, diluted in sterile PBS from a 20 mM stock; and 200 nM 1400W dihydrochloride (SW1400, MedChemExpress, HY-18730), a specific inhibitor of *iNos*, diluted in sterile PBS from a 39.97 mM stock. PBS was used as the control. Each solution was loaded into glass capillaries prepared using a micropipette puller (Narishige, PC-10) and connected to a microinjector (Applied Scientific Instrumentation, MPPI-3). Intraocular injection of the inhibitor solutions were administered to the zebrafish eyes starting 2 days before G/R cone ablation and continued until 72 hpi **(Figure 4C)**.

Additionally, zebrafish were pre-treated with 10 mM of the NO scavenger, Phenyl-4,4,5,5-tetramethyl imidazoline-1-oxyl 3-oxide (C-PTIO, Sigma-Aldrich, P5084-25MG), diluted in standard water (from a 100 mM stock), or dexamethasone (Dex, Sigma-Aldrich, D1756) which diluted in DMSO, starting 2 days before G/R cone ablation and continuing until 72 hpi **(Figure 2J and 4C)**.

The real-time quantitative PCR after FACS-sorted MG

We crossed *Tg(lws2: nfsb-mCherry)* with *Tg(pcna: GFP)*, *Tg(her4.1: dRFP)*, *Tg(gfap: EGFP)*, and *Tg(cxcl18b: GFP)* to collect retina cell. the retinas were

dissected and the cells dissociated for sorting and enrichment of signal-positive cells using fluorescence-activated cell sorting (FACS, Beckman, MoFlo XDP). After 72 hours post G/R cone ablation, GFP^+/RFP^+ cells were collected from the retinas of *Tg(lws2: nfsb-mCherry* x *pcna: GFP)* as the proliferative MG group. For the uninjured MG group, GFP^+/RFP^+ cells were collected from *Tg(lws2: nfsb-mCherry* x *gfap: EGFP* x *her4.1: dRFP)* uninjured retinas, while GFP^+/RFP^+ cells from injured retinas represented the 72-hpi MG group, while GFP^-/RFP^- cells were enriched as the other retinal cell types group in the 72 hpi retinas. Additionally, from *Tg(lws2: nfsb-mCherry* x *cxcl18b: GFP)* retinas, GFP^+/RFP^+ cells were collected as the *cxcl18b*$^+$ MG group and single RFP^+ cells as the G/R cone group at 72 hpi **(Figure 5A)**.

Interesting cells were collected into a 1.5 ml tube containing lysis buffer (20 mg/ml PK in TE buffer) and total RNA was isolated using this lysis buffer. cDNA synthesis was conducted by adding RT mix contains: 200 U Superscript II reverse transcriptase (Invitrogen, 18064 014), 1 × First strand buffer (Invitrogen, 18064 014), 5 mM DTT (Invitrogen, 18064 014), 20 U Recombinant RNase inhibitor (Clontech, 2313A), 6 mM MgCl2 (Sigma, M8266), 1 μM TSO**(Picelli et al., 2013)**; 8% PEG8000 (Sigma, P1458). PCR amplification was performed as previously described**(Picelli et al., 2013)**.

Real-time quantitative PCR (RT-qPCR) reactions were carried out using TB Green Premix Ex Taq (Takara, RR420A) on a LightCycler 480 II real-time PCR detection system (Roche). The qPCR primers are listed in **Supplementary Table S3**. The ΔΔCt method was used to determine the relative expression of mRNAs in different group retinae cells and normalized to *actin* mRNA levels. Each group comparison was performed using a two-way ANOVA followed by Tukey's HSD test. Error bars represented SEM. ****$p<0.0001$, ***$p<0.001$; **$p<0.01$; *$p<0.05$; ns, $p>0.05$.

Construction and injection of adenoviral-based MG-specific knockout system in the zebrafish retina

The type of AdC68 used in our study is a replication-deficient chimpanzee

adenovirus. The plasmids used for viral packaging were described above, and the amplification and purification of recombinant chimpanzee adenovirus followed the standard protocol**(Jia et al., 2019; Liu et al., 2021)**. We generated four adenoviruses for this study, including *AdC68XY2-E1-CMV-GFP pAdC68XY2-E1-10xUAS: Cas9-2a-Cre-U6: sgRNA1(nos2b)*; *U6: sgRNA2(nos2b)* (referred to as *UAS: Cas9-2a-Cre-sgnos2b*, infectious titer: 2.00 x 10^{13} ifu/ml), *pAdC68XY2-E1-cxcl18b: gal4FF* (referred to as *cxcl18b: gal4*, infectious titer: 1.90 x 10^{13} ifu/ml) and *pAdC68XY2-E1-10xUAS: Cas9-2a-Cre-U6: empty* (referred to as *UAS: Cas9-2a-Cre*, infectious titer: 1.75 x 10^{13} ifu/ml) as a control.

All adenoviruses were diluted in sterile PBS to a final infectious titer: 1.00 x 10^{13} ifu/ml. The *UAS: Cas9-2a-Cre-sgnos2b* and *cxcl18b: gal4* adenoviruses were mixed at a 1:1 ratio for the MG-specific knockout system, while the *UAS: Cas9-2a-Cre* with *cxcl18b: gal4* adenoviruses were similarly mixed as a control. To achieve the *cxcl18b*$^{+}$ MG cell-specific knockout *nos2b*, we performed the intraocular injection of the adenovirus mixtures into the eyes of *Tg(ef1α: loxP-DsRed-loxP-EGFP* x *lws2: nfsb-mCherry)* at 5 dpf. One day post-injection, the fish were treated with MTZ for 3 consecutive days to ablate the G/R cone **(Figure 6E)**.

Tissue preparation and immunostaining

Zebrafish were fixed in 4% paraformaldehyde (PFA, Electron Microscopy Services, 157–8) overnight, then cryoprotected in 30% sucrose for 6 hours, flash-frozen, and cryosectioned at a thickness of 14 μm. Immunostaining was performed following the protocol described by Tang et al.**(Tang et al., 2017)**. The primary antibody including mouse anti-PCNA (Abcam, ab29) at a 1:500 dilution, as well as mouse anti-GS (glutamine synthase, BD Transduction Laboratories, 610518), rabbit anti-BLBP (Abcam, ab32423), rabbit anti-DsRed (Clontech, 632496), rabbit anti-TaqGFP (Proteintech, 50430-2-AP), and chicken anti-GFP (Abcam, ab13970) each at a 1:1000 dilution. Secondary antibodies conjugated to Alexa Fluor 488, 594, or 647 (Jackson ImmunoResearch Laboratories Inc.) were used at a 1:1000 dilution. Primary antibodies were incubated overnight at 4°C, while Alexa Fluor secondary antibodies

were incubated at room temperature for 2 hours. DAPI staining was performed according to the standard protocol.

In situ hybridization

In this study, three digoxigenin (DIG)-labeled RNA probes targeting endogenous *cxcl18b*, *fabp11a*, and *col15α1b* were synthesized using the MEGAscript™ T7 High Yield Transcription Kit (Invitrogen, AM1334) and the DIG RNA Labeling Kit (Roche, 11277073910), following the manufacturer's instructions. The cDNA of each gene was amplified by PCR using the following primers: *cxcl18b* -F: 5'-ATGGCATTCACACCCAAAGCG-3'; *cxcl18b* -R: 5'-TAATACGACTCACTATAGGGATTGGCCCTGCTGTTTTTGTG-3'; *fabp11a*-F: 5'-GTTGGAAACCGGACCAAACC-3'; *fabp11a*-R: 5'-TAATACGACTCACTATAGGGACGGCTCGTTGAGCTTGAAT-3'; *col15a1b* -F: 5'-CCTCAATGGAGGTCCTAAAGGT-3'; *col15α1b* -R: 5'-TAATACGACTCACTATAGGGACCAGCTTCTGAGACCAAGC-3'.

Following the *in situ* hybridization protocol described by Tang et al.**(Tang et al., 2017)**, fresh zebrafish retinal sections were incubated overnight in the HybEZ system (Advanced Cell Diagnostics, 310013) at 65°C with 200 ng of probe for each slide. The next day, slides were sequentially washed in 5x SSC buffer and incubated overnight at 4°C with an anti-DIG-POD antibody (Roche, 11093274910) diluted 1:500 in TNB buffer (TN buffer with 0.5% blocking reagent; Roche). On the third day, the signal was detected using the TSA™ Plus Cyanine 3 (PerkinElmer, NEL744001KT) or Cyanine 5 (PerkinElmer, NEL745001KT)/Fluorescein System.

Imaging

Images were taken using an inverted confocal microscope system (FV1200, Olympus) confocal microscope using 40 × (silicon oil, 1.05 NA), or 60 × (silicon oil, 1.3 NA) objectives.

Quantifications and statistical analysis

All quantification and visualization were performed with FV31S-SW 2.3.1.163 Viewer (Olympus), and ImageJ. ***Z intensity projection*** was used to process the Z-stack images acquired from 14-μm-thick sections of zebrafish retina for statistical analysis. For cell counting, PCNA^{+} MG and their lineage in this study were defined as one proliferative MG, *cxcl18b*$^{+}$ MG and their lineage were counted as one *cxcl18b*$^{+}$ MG.

To perform the statistical analysis, p values were calculated with GraphPad Prism 8 (or Microsoft Excel). The unpaired, non-parametric Wilcoxon test was applied for comparison of two groups. The one-way ANOVA, followed by Tukey's HSD test was applied for comparison of different groups with one treatment. The two-way ANOVA followed by Tukey's HSD test was applied for comparison of four groups with two treatments. Error bars represent SEM. ****$p<0.0001$, ***$p<0.001$; **$p<0.01$; *$p<0.05$; ns, $p>0.05$.

Main Figure Titles and Legends

Figure 1. Single-cell RNA seq reveals injury-induced the *cxcl18b*-defined MG transitional states

(A) Schematic showing the experimental procedure: five consecutive days of MTZ treatment in *Tg(lws2: nfsb-mCherry* x *mpeg1: GFP)* fish to ablate green and red (G/R) cone, starting at 6 dpf and continuing until 11 dpf. The MTZ solution was refreshed every 24 hours, followed by fish fixation for further immunostaining.
(B-D) Quantitative plots showing the dynamic changes in the number of G/R cone **(B)**, recruited microglia **(C)**, and proliferative MG ($PCNA^+$) **(D)** at different time points after MTZ treatment (uninjured: collected retina number n=14; 24-hpi: n=10; 48-hpi: n=10; 72-hpi: n=11; 96-hpi: n=12; 120-hpi: n=16; mean ± SEM; ****p<0.0001, ***p<0.001, **p<0.01, ns, p>0.05; one-way ANOVA followed by Tukey's HSD test).
(E) Representative images showing microglia recruitment (*mpeg1: GFP*, green), G/R cone ablation (*lws2: nfsb-mCherry*, red), and injury-induced MG proliferation (PCNA, white) in uninjured **(E_1)** and 72-hpi **(E_2)** retinas. The high-magnification images of the boxed area **(E_3-E_4)**. Scale Bars: 20□μm **(E_1, E_2)**, 10□μm **(E_3)**, 2□μm **(E_4)**.
(F) The UMAP plot of 4,172 MG cells was sorted with an increased proportion in response to the G/R cone ablation. Cells were further aggregated into 10 clusters based on previously published scRNA-seq data**(Krylov et al., 2023)**.
(G) Pseudo-time developmental trajectory of MG states identified by Monocle2 analysis shows a main developmental branch originating from Cluster 4 (*cx43*$^+$), which diverges into two sub-branches: Cluster 0 and Clusters 5/3/6 (*pcna*$^+$).
(H) Violin plots showing the expression levels of key genes (*cx43*, *glula*, *gfap*, *cxcl18b*, *ascl1α*, *mki67*, *pcna*, and *notch3*) in the main developmental branch clusters, progressing from the most original MG states (Cluster 4) to transitional MG states (Clusters 1/2/5), and proliferative MG states (Clusters 3/6).

Figure 2. Clonal analysis reveals the proliferative MG mostly originated from *cxcl18b*$^+$ MG transitional states

(A) Representative images show dynamic expression of *cxcl18b* (red, *in situ* hybridization) and PCNA (white, immunostaining) in *Tg(lws2: nfsb-mCherry)* retina at different time points following the G/R cone ablation. Scale bars: 20 μm.
(B) Quantitative plots showing the number of *cxcl18b*$^+$ (red curve, significance shown above the curve) and $PCNA^+$ MG (blue curve, significance shown below the curve) in uninjured (n=11) and injured retina at 24-hpi (n=10), 48-hpi (n=12), 72-hpi (n=11), 96-hpi (n=7), and 120-hpi (n=5). Each injured time point was compared to the uninjured retina (Mean ± SEM; ****p<0.0001, **p<0.01, ns, p>0.05; one-way ANOVA followed by Tukey's HSD test).
(C) Schematic diagram of the *cxcl18b* promoter was used to construct the reporter

fish line *Tg(cxcl18b: GFP)* and clonal analysis fish line *Tg(cxcl18b: Cre-vmhc-mCherry:: ef1α: loxP-DsRed-loxP-EGFP; lws2: nfsb-mCherry)*.

(D) Immunostaining of injury-induced *cxcl18b*$^+$ (green, indicated by *Tg(cxcl18b: GFP)*) and proliferative (PCNA$^+$, white) MG showing overlapping in the central retina area (yellow arrows, GFP$^+$/PCNA$^+$ MG) at 48 hpi. The high-magnification images of the boxed area **($D_{3'}$-$D_{3'''}$)**. The area of the retina is labeled with a dashed line, and each layer structure is labeled with dashed lines and marked with the outer nuclear layer (ONL), inner nuclear layer (INL), inner plexiform layer (IPL), ganglion cell layer (GCL) and lens. Scale Bars: 20□μm **(D_1-D_2)** and 5 μm **($D_{3'}$-$D_{3'''}$)**.

(E) Quantitative plots showing the number of *cxcl18b*$^+$ MG (red) and proliferative MG (PCNA$^+$, blue) in **(D_1)** uninjured (n=4) and **(D_2)** 48-hpi retina (n=7) (Mean ± SEM; ****p<0.0001, ns, p>0.05; two-way ANOVA followed by Tukey's HSD test).

(F) Clonal analysis of injury-induced *cxcl18b*$^+$ MG in transgenic fish line *Tg(cxcl18b: Cre-vmhc: mCherry:: ef1α: loxP-DsRed-loxP-EGFP:: lws2: nfsb-mCherry)* at 72 hpi retina showing overlapping between proliferative (PCNA$^+$, white) MG with *cxcl18b*$^+$ (green, yellow arrows). The high-magnification images of the boxed area **($F_{3'}$-$F_{3'''}$)**. Scale Bars: 20□μm **(F_1-F_2)** and 5 μm **($F_{3'}$-$F_{3'''}$)**.

(G) Quantitative analysis at 72 hpi shows no significance in the number of proliferative MG (PCNA+, blue) and double-positive (PCNA$^+$ / *cxcl18b*$^+$, red) MG (n=14; Mean ± SEM; ns, p>0.05; Unpaired t-test) in **(F)**, with 93±2% of PCNA$^+$ MG also being *cxcl18b*$^+$.

(H) Representative images show that not all mature MG stained with glutamate synthase (GS$^+$, magenta) are *cxcl18b*$^+$ (green, labeled by *cxcl18b*: Cre) in the central retinal area (white dashed lines identified a 45° angular region originating from the optic nerve). The high-magnification images of the boxed area **($H_{2'}$-$H_{2'''}$)**. Scale Bars: 20□μm **(H_1)** and 5 μm **($H_{2'}$-$H_{2'''}$)**.

(I) Quantification of GS$^+$/*cxcl18b*: Cre$^+$ double-positive (blue, yellow arrows in **H**) and GS$^+$/*cxcl18b*: Cre$^-$ single-positive (red, open yellow arrowheads in **H**) MG (n=14, Mean ± SEM; *p<0.05; one-way ANOVA followed by Tukey's HSD test), and the proportion of *cxcl18b*: Cre$^{+\text{ or }-}$ MG within the total population of mature (GS$^+$) MG in the central retina.

(J_1-J_3) Representative images showing injury-induced *cxcl18b*$^+$ MG (green) in *Tg(lws2: nfsb-mCherry x cxcl18b: GFP)* fish retina treated with dexamethasone (Dex) or DMSO at 72 hpi. Scale bars: 20 μm.

(K-M) Quantitative plots showing the number of *cxcl18b*$^+$ MG (72 hpi: n=14; DMSO: n=6, Dex: n=10) in **J_1-J_3**; recruited microglia in **Figure 2-figure supplement 1J_1-J_3** and proliferative MG in **Figure 2-figure supplement 1J_4-J_6** (72 hpi: n=9; DMSO: n=7, Dex: n=14) in *Tg(mpeg1: GFP; lws2: nfsb-mCherry)* retinas after DMSO or Dex treatment at 72 hpi (Mean ± SEM; ****p<0.0001, ***p<0.001, ns, p>0.05; one-way ANOVA followed by Tukey's HSD test).

Figure 3. The *cxcl18b*-defined MG transitional states recapitulate the developmental states of RSCs in the CMZ

(A, C) UMAP plots display 5,368 retinal progenitor cells (RPCs) at 24 hpf and 4,625 CMZ progenitor cells at 14 dpf. Clusters are indicated by their cluster-specific marker genes based on previously published scRNA-seq data**(Xu et al., 2020)**.

(B, D) UMAP plots showing expression of *fabp11a*, *cxcl18b*, and *col15α1b* at r24-hpf RPCs (embryonic states) **(B)** and r14-dpf CMZ-progenitors (post-embryonic states) **(D)**.

(E-H_3) *In situ* hybridization images showing the expression of *fabp11a* (green), *col15α1b* (white), two putative makers for post-embryonic retinal stem cells (RSCs), and *cxcl18b* at 30-hpf **(E-F_3)** and 14-dpf **(G-H_3)** retina. The high-magnification images of the boxed area **(F-F_3, H-H_3)**. The area of these three in situ signal trouble positive is labeled with a dashed yellow line. Scale Bars: 20 μm **(E, G)** and 3 μm **(F-F_3, H-H_3)**.

Figure 4. The nitric oxide metabolic pathway regulates injury-induced MG proliferation

(A) Representative images of microglia recruitment (green, marked by *Tg(mpeg1: GFP)*), G/R cone ablation (red, marked by *Tg(lws2: nfsb-mCherry)*) and proliferative MG (white, marked by $PCNA^+$) at 72 hpi with nitric oxide metabolism pathway genes disruption (*nos1*/*nos2a*/*nos2b*/*gsnor*). Scale Bars: 20 μm.

(B) Quantitative analysis of the number of proliferative MG ($PCNA^+$) at 72 hpi in **(A)**. In total, we collected 11 retinas for WT (n=11), *scramble* sgRNA-injection (n=7), *nos1* sgRNA-injection (n=23), *nos2a* sgRNA-injection (n=15), *nos2b* sgRNA-injection (n=22), and *gsnor* sgRNA-injection (n=13) (Mean ± SEM; ****$p<0.0001$, **$p<0.01$, *$p<0.05$, ns, $p>0.05$; one-way ANOVA followed by Tukey's HSD test).

(C) Schematic showing the experimental procedure of nitric oxide synthase (*Nos*) inhibitors injection or NO scavengers treatment in *Tg(lws2: nfsb-mCherry* x *mpeg1: GFP)* retina starting from 5 dpf for five consecutive days to 10 dpf with three consecutive days of MTZ treatment for G/R cone ablation from 7 dpf to 10 dpf. *Nos* inhibitors, NO scavengers, and MTZ solution were refreshed every 24 hours, and fish fixation was at 10 dpf for further immunostaining.

(D) Representative images of microglial recruitment (green, marked by *Tg(mpeg1: GFP)*), G/R cone ablation (red, marked by *Tg(lws2: nfsb-mCherry)*) and proliferative MG (white, marked by $PCNA^+$) at 72 hpi following L-NMMA (10 mM), L-NAME (10 mM), 1400W (200 nM) intraocular injection, and PBS as control, or C-PTIO (10 mM) treatment. Scale Bars: 20 μm.

(E) Quantitative plots showing the number of proliferative ($PCNA^+$) MG at 72 hpi in **(D)**. Retinas analyzed WT (n=11), PBS-injected (n=16), L_NMMA-injected (n=12), L_NAME-injected (n=12), 1400W-injected (n=10), and C-PTIO treatment (n=27) (Mean ± SEM; ****$p<0.0001$, ns, $p>0.05$; one-way ANOVA followed by Tukey's HSD test).

(F-G) Representative images of proliferative MG ($PCNA^+$, white) and G/R cone ablation (marked by *Tg(lws2: nfsb-mCherry)*, red) at 72 hpi in heterozygous (*nos1*$^{+/-}$,

nos2a$^{+/-}$, *nos2b*$^{+/-}$, *gsnor*$^{+/-}$) **(F)** and homozygous mutants **(G)** of nitric oxide metabolism pathway genes (*nos1*$^{-/-}$, *nos2a*$^{-/-}$, *nos2b*$^{-/-}$, *gsnor*$^{-/-}$). Scale Bars: 20 μm.

(H-I) Quantitative plots showing the number of proliferative MG (white, PCNA^{+}) at 72 hpi in *nos* and *gsnor* mutant fish. In heterozygous **(H)**, analyzed retinas include WT (n=14), *nos1*$^{+/-}$ (n=19), *nos2a*$^{+/-}$ (n=13), *nos2b*$^{+/-}$ (n=20), *gsnor*$^{+/-}$ (n=12). For homozygous **(I)**, analyzed retinas include *nos1*$^{-/-}$ (n=18), *nos2a*$^{-/-}$ (n=20), *nos2b*$^{-/-}$ (n=20), *gsnor*$^{-/-}$ (n=27) (Mean ± SEM; ****p<0.0001, ns, p>0.05; one-way ANOVA followed by Tukey's HSD test).

(J-K) Quantitative plots showing the number of proliferative MG (white, PCNA^{+}) **(J)** and photoreceptor cells remain **(K)** at 72 hpi in *nos2b* hetero- or homozygous mutants. (Mean ± SEM; ****p<0.0001, ***p<0.001, ns, p>0.05; one-way ANOVA followed by Tukey's HSD test).

Figure 5. RT-qPCR analysis reveals *nos2b* cell-specific expression in the injury-induced *cxcl18b*$^{+}$ MG

(A) Schematic showing the workflow for isolating and enriching for three post-injury MG populations (72-hpi MG, 72-hpi PCNA^{+} MG, and 72-hpi *cxcl18b*$^{+}$ MG) and three control groups (uninjured MG, 72-hpi retinal cells other than MG, and 72-hpi G/R cones) using fluorescence-activated cell sorting (FACS).

(B-C) RT-qPCR analysis of *nos1*, *nos2a*, *nos2b*, and *gsnor* expression in different cell populations. Expression levels are shown relative to 72-hpi G/R cones **(B)** and other 72-hpi retinal cell types **(C)**. A total of six independent replicates were performed for cell population enrichment and cDNA template preparation (n=6, Mean ± SEM; ****p<0.0001, ns, p>0.05; two-way ANOVA followed by Tukey's HSD test).

(D) RT-qPCR analysis comparing *nos1*, *nos2a*, *nos2b*, and *gsnor* expression in distinct MG states relative to uninjured MG (repeats n=7 in *cxcl18b*$^{+}$ MG; n=5 in 72-hpi MG; and repeats n=6 in PCNA^{+} MG; n=6 in the uninjured retina; Mean ± SEM; ****p<0.0001, ns, p>0.05; two-way ANOVA followed by Tukey's HSD test).

Figure 6. NO produced by *nos2b* in *cxcl18b*$^{+}$ MG regulates injury-induced proliferation

(A-C) Representative images showing the adenovirus-mediated infection (green, indicated by Y_2-GFP) specifically target MG (red, GS staining) in the zebrafish retina. The virus was intraocularly injected into the right eye of *Tg(lws2: nfsb-mCherry* x *ef1α: loxP-DsRed-loxP-EGFP)* fish **(A_2, C)**, with the left eye as a wild-type (WT) control **(A_1)**. The high-magnification images of the boxed area (B-B_3). Scale Bars: 20 μm (A_1, A_2) and 5 μm (B-B_3).

(D) Schematic showing the design of the *cxcl18b*$^{+}$ MG-specific *nos2b* knockout system. The viral construct consists of three plasmids: (1) *gal4* expression driven by the *cxcl18b* promoter; (2) *UAS*-derived *Cas9* and *Cre* elements, and (3) *U6* promoters

driving two sgRNAs targeting *nos2b*, with a non-targeting sgRNA as the control.
(E) Schematic showing the procedure of injury process and intraocular viral injection in *Tg(lws2: nfsb-mCherry* x *ef1α: loxP-DsRed-loxP-EGFP)* fish.
(F-G) Representative images showing proliferative MG ($PCNA^+$, white) with *cxcl18b*$^+$ MG specific knockout *nos2b* in **(G)** and control in **(F)**, (GFP^+, green, yellow arrows) are defined as virus-infected clones. Upper panels show WT retina (no virus injected),
Bottom panels show retinas injected with the virus (two sgRNA targets as *nos2b* knockout and without sgRNA targets as control). Scale Bars: 20 μm.
(H) Quantification of proliferative ($PCNA^+/GFP^+$, red bars) and non-proliferative ($PCNA^-/GFP^+$, gray bars) MG clones in (**F**). For control, ~75% of virus-infected clones entered the cell cycle ($PCNA^+$; red bars), with 90/120 clones analyzed across 8 independent experiments (n=8). For *nos2b* knockout clones, ~23% entered the cell cycle ($PCNA^+$; blue bars), with 22/103 clones analyzed across 6 independent experiments (n=6) (Mean ± SEM; ****p<0.0001; two-way ANOVA followed by Tukey's HSD test).

Figure 7. NO regulates MG proliferation by suppressing Notch signaling

(A) Dot plot showing the Notch signaling-related gene expression in different MG states. The average expression levels of these genes for all cells in each cluster are coded by the gray level. The percentage of cells expressing each gene within each cluster is coded by dot size.
(B) Representative images showing the dynamic changes of Notch signaling activity (green, indicated by *Tg(Tp1: EGFP)*) and proliferative MG (white, $PCNA^+$) following injury with nitric oxide (NO) blockade using C-PTIO. Scale Bars: 20 μm.
(C-D) Quantitative plots showing the number of Notch activation (*tp1*: GFP^+ MG) in **(C)** and proliferative MG ($PCNA^+$ MG) in **(D)** at different time points post-G/R cone ablation. We collected uninjured retina (24-hpi, n=4; 48-hpi, n=4; 72-hpi, n=3), injured retina (24-hpi, n=9; 48-hpi, n=4; 72-hpi, n=6), and retina treated with C-PTIO (24-hpi, n=6; 48-hpi, n=5; 72-hpi, n=7) (Mean ± SEM; ****p<0.0001, ***p<0.001, **p<0.01, *p<0.05, ns, p>0.05; two-way ANOVA followed by Tukey's HSD test).

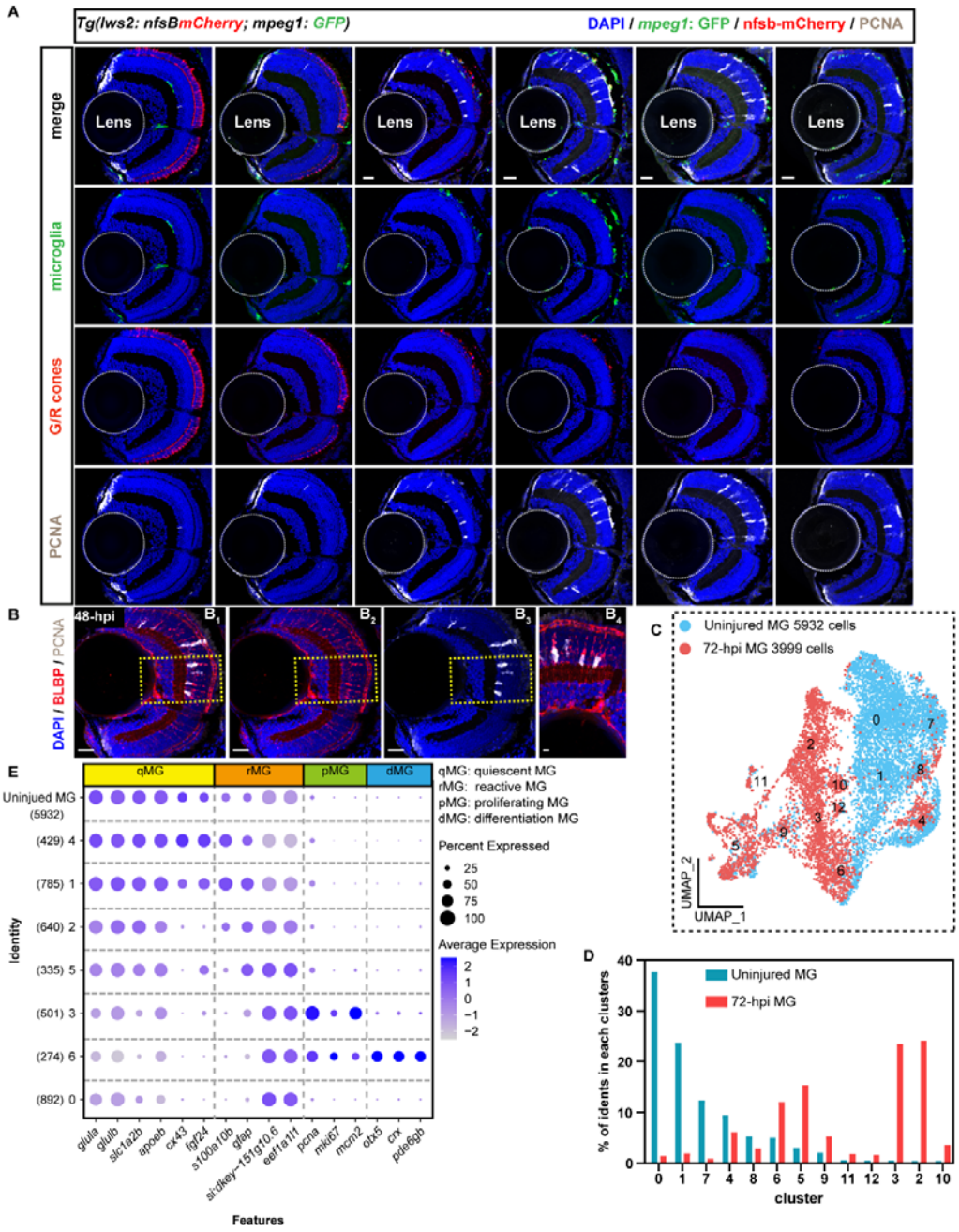

Figure 1-figure supplement 1. Clusters with increased proportion are identified from the scRNA-seq data

(A) Representative images showing microglia recruitment (green, indicated by *Tg(mepg1: GFP)*), G/R cone ablation (red, *Tg(lws2: nfsb-mCherry)*), and injury-induced MG proliferation (white, marked by PCNA) following the injury process from uninjured retina to 120 hpi. Scale Bars: 20□μm.

(B) Representative images showing PCNA+ (white, immunostaining) cells co-expressed with BLBP (red, immunostaining) at 72 hpi. Scale Bars: 20□μm (B_1-B_3)

and 5 μm **(B_4)**.

(C) UMAP plot showing 5,932 cells from uninjured retinas (blue) and 3,999 cells from 72-hpi (red) retinas were obtained, which were further aggregated into 13 clusters.

(D) Percentage of MGs from uninjured and 72-hpi retinas in each cluster. Eight clusters (6, 5, 9, 11, 12, 3, 2, 10) were identified and showed an increased proportion for further analysis.

(E) Dot plot showing the expression levels of marker genes for quiescent MG (qMG), reactive MG (rMG), proliferative MG (pMG), and differentiated MG (dMG). The average expression levels of these genes for all cells in each cluster are coded by the gray level. The percentage of cells expressing each gene within each cluster is coded by dot size.

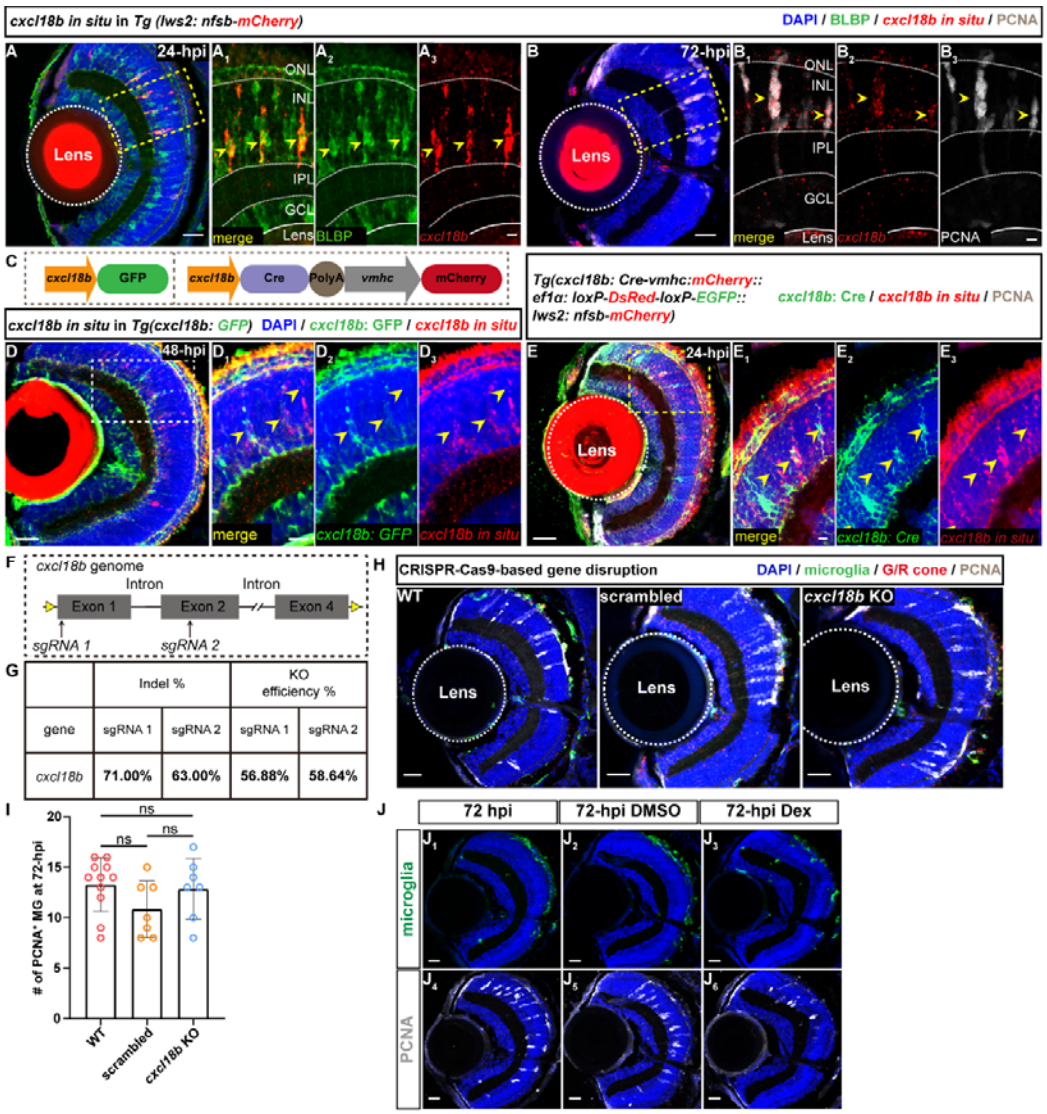

Figure 2-figure supplement 1. Gene description of *cxcl18b* does not reduce MG proliferation

(A-A$_3$) *In situ* hybridization images show injury-induced *cxcl18b* (red, marked by *in situ* hybridization) with MG-like morphology, cell-specific expression in the BLBP$^+$ cells (green, labeled by immunostaining) at 24 hpi in the transgenic fish line *Tg(lws2: nfsb-mCherry)* retina. In these clones, *cxcl18b*$^+$ MG are red$^+$/BLBP$^+$ cells (yellow arrowheads). The high-magnification images of the boxed area **(A$_1$-A$_3$)**. The area of the retina structure is labeled with a dashed line, and each layer structure is labeled with dashed lines and marked with the outer nuclear layer (ONL), inner nuclear layer (INL), inner plexiform layer (IPL), ganglion cell layer (GCL), and lens. Scale Bars: 20 μm **(A)** and 5 μm **(A$_1$-A$_3$)**.

(B-B$_3$) Representative images showing *cxcl18b* (red, *in situ* hybridization) co-expressed with PCNA (white, immunostaining) at 72 hpi. In these clones, *cxcl18b*$^+$

MG was identified as red$^+$/PCNA$^+$ cells (yellow arrowheads). The high-magnification images of the boxed area **(B_1-B_3)**. Scale Bars: 20 μm **(B)** and 5 μm **(B_1-B_3)**.

(C) Schematic showing the design of the *cxcl18b* reporter fish line and the Cre-loxP transgenic fish line used for clone analysis. The *cxcl18b* promoter drives GFP or Cre expression, with the heart labeled by mCherry under the *vmhc* promoter for fish screening.

(D-E_3) Representative images showing *cxcl18b* expression labeled by *Tg(cxcl18b: GFP)* (green) in **(D-D_3)** at 48 hpi, or three transgenic fish *Tg(cxcl18b: Cre-vmhc: mCherry:: ef1α: loxP-DsRed-loxP-EGFP:: lws2: nfsb-mCherry)* (green) in **(E-E_3)** at 24 hpi fish retina, merged with *cxcl18b* in situ hybridization signal (red) **(D-E_3)**. The high-magnification images of the boxed area **(D_1-D_3, E_1-E_3)**. Scale Bars: 20 μm **(D, E)** and 5 μm **(D_1-D_3, E_1-E_3)**.

(F) Schematic showing the two sgRNA target sites of the *cxcl18b* genome.

(G) Summary table showing the indel and knockout efficiency of the two sgRNAs targeting *cxcl18b*.

(H) Representative images of proliferative MG (PCNA$^+$, white) at 72 hpi in *Tg(lws2: nfsb-mCherry)* fish retina with *cxcl18b* disruption. Scale Bars: 20 μm.

(I) Quantitative plots showing the number of proliferative MG (PCNA$^+$) at 72 hpi in **H**. In total, retinas were collected from wild-type (WT, n=11), *scramble* sgRNA-injected (*scrambled*, n=7), and *cxcl18b* sgRNA-injected (*cxcl18b* KO, n=7) (Mean ± SEM; ns, p>0.05; one-way ANOVA followed by Tukey's HSD test).

(J_1-J_6) Representative images showing injury-induced microglia recruitment (green, marked by *Tg(mpeg1: GFP)*) **(J_1-J_3)**, and proliferative MG (white, marked by PCNA) **(J_4-J_6)** after dexamethasone (Dex) or DMSO treatment in the in *Tg(mpeg1: GFP x lws2: nfsb-mCherry)* fish retina at 72 hpi. Scale bars: 20 μm.

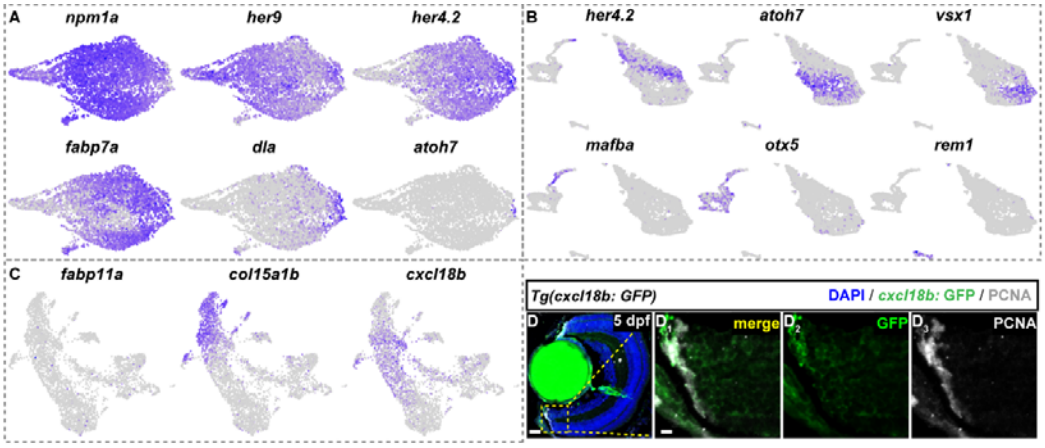

Figure 3-figure supplement 1. UMAP plots show the expression of cluster-specific marker genes utilized to identify developmental states

(A, B) UMAP plots showing the expression pattern of embryonic developmental stage cluster-specific marker genes (*npm1a*, *her9*, *her4.2*, *fabp7a*, *dla*, and *atoh7*) in **(A)** and post-embryonic developmental stage marker genes (*her4.2*, *atoh7*, *vsx1*, *mafba*, *otx5*, and *rem1*) in **(B)**.
(C) UMAP plots showing the expression pattern of *fabp11a*, *cxcl18b*, and *col15α1b* at MG clusters with increased population after G/R cone ablation at 72 hpi in Figure 1F.
(D) Representative images showing the *cxcl18b* expression (green, marked by *Tg(cxcl18b: GFP)*) are located in the most peripheral region of the CMZ (white, marked by PCNA) at 5 dpf. The high-magnification images of the boxed area **(D_1-D_3)**. Scale Bars: 20 μm **(D)** and 5 μm **(D_1-D_3)**.

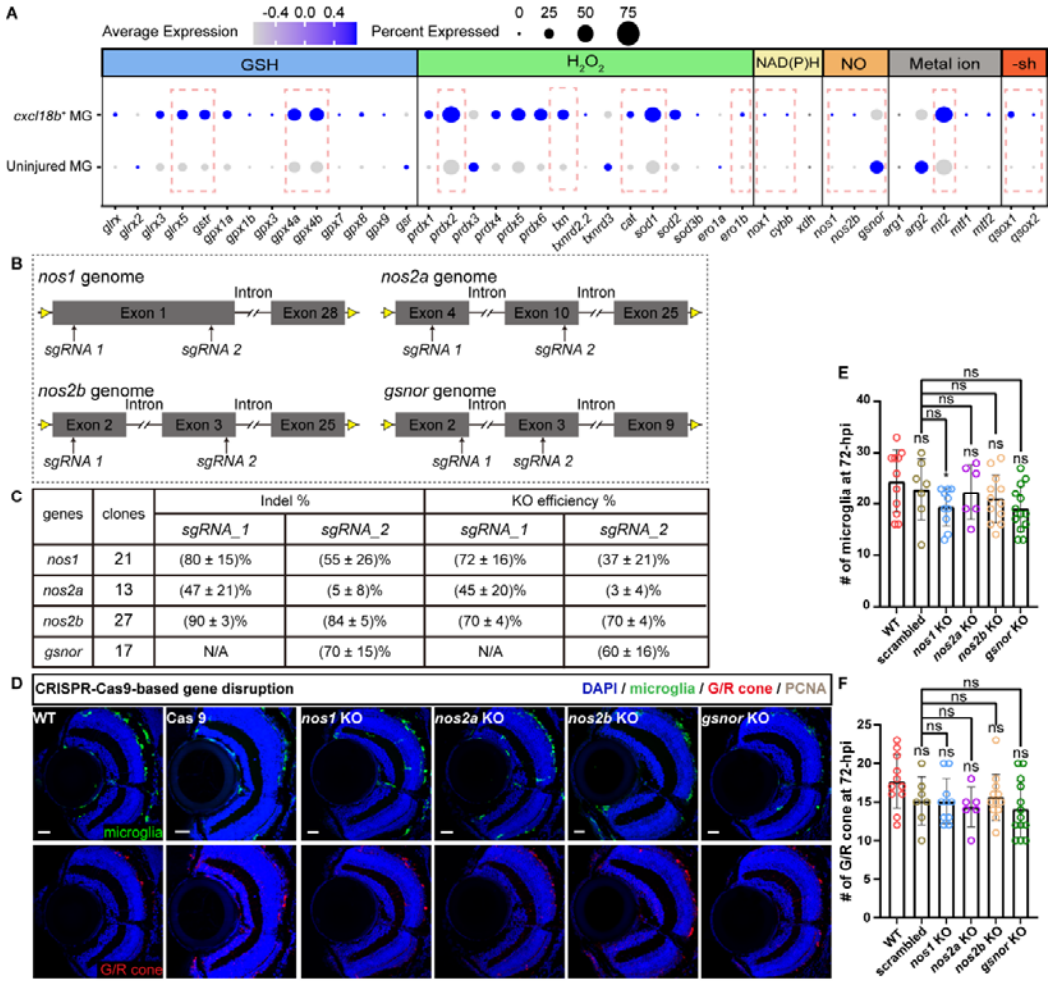

genes	clones	Indel %		KO efficiency %	
		sgRNA_1	*sgRNA_2*	*sgRNA_1*	*sgRNA_2*
nos1	21	(80 ± 15)%	(55 ± 26)%	(72 ± 16)%	(37 ± 21)%
nos2a	13	(47 ± 21)%	(5 ± 8)%	(45 ± 20)%	(3 ± 4)%
nos2b	27	(90 ± 3)%	(84 ± 5)%	(70 ± 4)%	(70 ± 4)%
gsnor	17	N/A	(70 ± 15)%	N/A	(60 ± 16)%

Figure 4-figure supplement 1. Genetic disruption of the nitric oxide pathway modulates G/R cone ablation and microglial recruitment

(A) Dot plot showing the redox gene expression profiles of regulating glutathione (GSH), hydrogen peroxide (H_2O_2), nicotinamide adenine dinucleotide phosphate (NADPH), nitric oxide (NO), metal ion, and sulfhydryl group (-SH) in the uninjured and *cxcl18b*$^+$ MG in 72-hpi scRNA-seq data **(Krylov et al., 2023)**. The average expression levels of these genes for all cells in each cluster were coded by the gray level. The percentage of cells expressing each gene within each cluster was coded by dot size.

(B) Schematic showing the two sgRNA target sites of the nitric oxide metabolism pathway genome (*nos1*/*nos2a*/*nos2b*/*gsnor*).

(C) Summary table showing the indel and knockout efficiency of the two sgRNAs targeting *nos1*/*nos2a*/*nos2b*/*gsnor*.

(D) Representative images of microglial recruitment (marked by *Tg(mpeg1: GFP)*, green) and G/R cone ablation (marked by *Tg(lws2: nfsb-mCherry)*, red) at 72 hpi with *nos1*/*nos2a*/*nos2b*/*gsnor* disruption, with *scrambled* sgRNA-injected as the control.

Scale Bars: 20 μm.

(E-F). Quantitative plots showing the number of recruited microglia (GFP^+) **(D)** and G/R cone ablation ($mCherry^+$) **(E)** at 72 hpi with *nos1*/*nos2a*/*nos2b*/*gsnor* disruption. In total, we collected 11 retinas for WT (n=11), *scrambled* sgRNA-injected (n=7), *nos1* sgRNA-injected (n=10), *nos2a* sgRNA-injected (n=6), *nos2b* sgRNA-injected (n=12), and *gsnor* sgRNA-injected (n=13) (Mean ± SEM; *$p<0.05$; ns, $p>0.05$; one-way ANOVA followed by Tukey's HSD test).

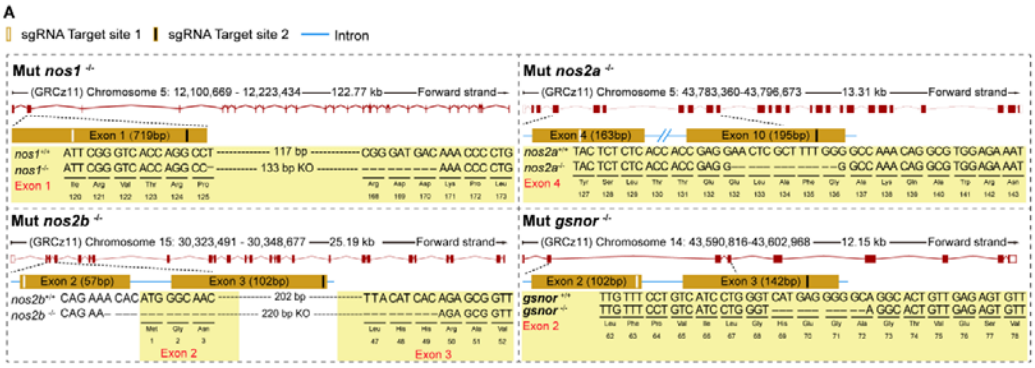

B

gene	AA	premature stop codon AA site	unknown polypeptides
nos1	1431	123	123-125
nos2a	1079	132	133-184
nos2b	1077	1	
gsnor	376	69	69-72

Figure 4-figure supplement 2. The genotype of nitric oxide metabolism pathway mutants

(A) Sequence alignment of WT nitric oxide metabolism pathway genes (*nos1*/*nos2a*/*nos2b*/*gsnor*) and their CRISPR-cas9-induced mutant alleles.

(B) Summary table showing the premature stop codon and unknown polypeptides sides of each mutant.

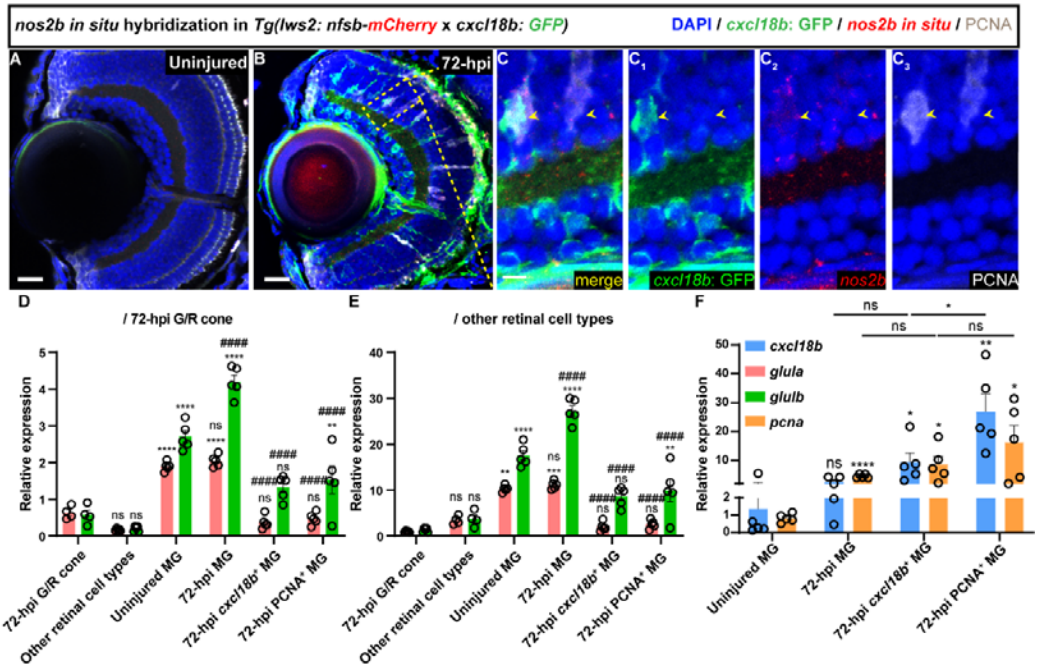

Figure 5-figure supplement 1. *In situ* hybridization reveals *nos2b* cell-specific expression in the *cxcl18b*-defined transitional MG states

(A-A$_3$) Representative *in situ* hybridization images showing *nos2b* expression (red, *in situ* hybridization) cell-specific in the injury-induced *cxcl18b*$^+$ MG (GFP$^+$, green) in *Tg(lws2: nfsb-mCherry* x *cxcl18b: GFP)* fish retina at 72 hpi. Clones with green/red/white trouble-positive are *cxcl18b*$^+$/*nos2b*$^+$/PCNA$^+$ MG cells (yellow arrowheads). The high-magnification images of the boxed area **(C-C$_3$)**. Scale Bars: 20 μm (A, B) and 5 μm **(C$_1$-C$_3$)**.

(D-E) RT-qPCR analysis of *glula* (pink bar) and *glulb* (green bar) expression in different cell populations relative to 72-hpi G/R cone **(D)**, or other retinal cell types **(E)**. The significance of 72-hpi G/R cone as control is noted by * for comparisons with 72-hpi G/R cones and # for comparisons with uninjured MG. In total, we do 6 independent replicates to enrich the different cell populations and get the cDNA templates (Mean ± SEM; **** and ####p<0.0001, **p<0.001, **p<0.01, ns, p>0.05; two-way ANOVA followed by Tukey's HSD test).

(F) RT-qPCR analysis of *cxcl18b* (blue bar) and *pcna* (orange bar) expression in different MG states. (Mean ± SEM; ****p<0.0001, **p<0.01, *p< 0.05, ns, p>0.05; two-way ANOVA followed by Tukey's HSD test).

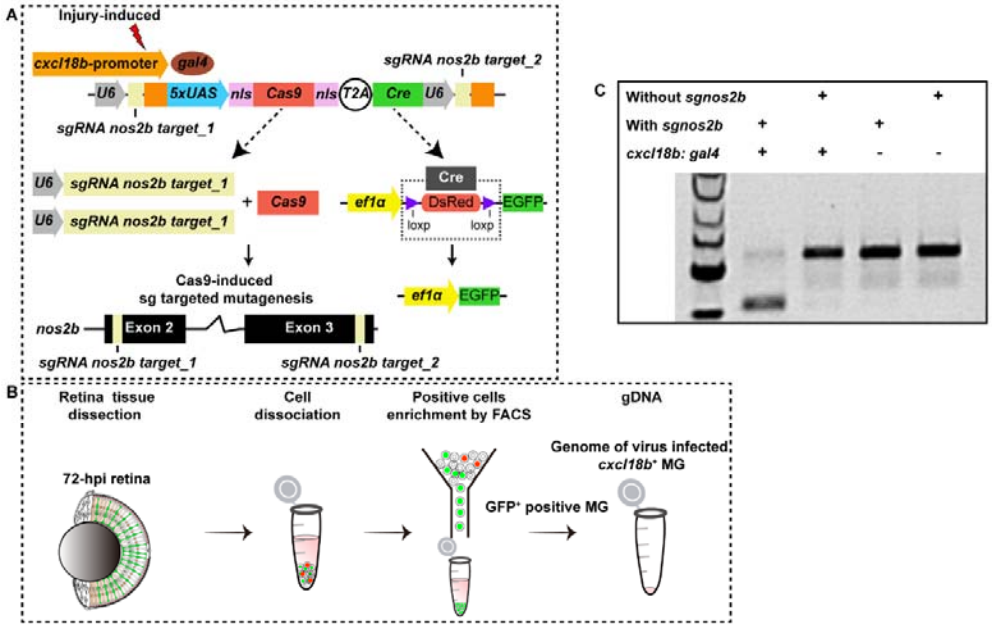

D

virus	clones	mutations	deletions	insertions	ORF shift	KO efficiency
With sgTarget + *cxcl18b: gal4*	26	18 (69.23%)	12 (46.15%)	12 (46.15%)	12 (46.15%)	12 (46.15%)
Without sgTarget + *cxcl18b: gal4*	27	1 (3.70%)	0 (0%)	0 (0%)	0 (0%)	1 (3.70%)
With sgTarget	25	1 (3.70%)	0 (0%)	0 (0%)	0 (0%)	0 (0%)
Without sgTarget	21	1 (3.70%)	0 (0%)	0 (0%)	0 (0%)	0 (0%)

Figure 6-figure supplement 1. Analysis of cell-specific knockout efficiency for *nos2b* in virus-infected clones

(A) Schematic showing the cell-specific gene knockout system design. Injury-induced *cxcl18b* promoter directs the expression of *gal4*, which in combination with the *UAS* element, drives the cell-specific expression of Cas9 and Cre. The *U6* promoter enables the broad expression of sgRNAs targeting *nos2b*, and Cas9 mediates gene knockout within the targeted cells through these sgRNAs. The *ef1α* promoter controls the *loxP-DsRed-loxP-EGFP* reporter system, allowing for the switch from DsRed to EGFP upon Cas9 and Cre activity, and GFP^+ MG clones are identified with successful *nos2b* knockout. This system operates with high specificity via double adenovirus infection.
(B) Schematic showing the procedure of virus-infected clones are sorted and enriched by FACS for further knockout efficiency analysis.
(C) Representative gel electrophoresis image showing *nos2b* deletions in knockout cells compared to controls. Single-virus injections were used to assess Cre system leakage. While minimal Cre system leakage was observed, it did not result in detectable *nos2b* knockout.
(D) Summary table showing the knockout efficiency of each virus-injected clone.

Supplementary Table S1. sgRNA sequences and genotyping primers, related to STAR Methods.

sgRNA targets sequences	
Gene symbol	**Primer forward**
nos1 sgRNA target-1	TAATACGACTCACTATAGGCTCCCAGGAAAGAGTCGCGTTTTAGAGCTAGAAATAGC
nos1 sgRNA target-2	TAATACGACTCACTATAGGTCACCAGGCCTGTCAACCGTTTTAGAGCTAGAAATAGC
nos2a sgRNA target-1	TAATACGACTCACTATAGGAGGAACTCGCTTTTGGGGGTTTTAGAGCTAGAAATAGC
nos2a sgRNA target-2	TAATACGACTCACTATAGGTGGCTGGTGCCACCGATGGTTTTAGAGCTAGAAATAGC
nos2b sgRNA target-1	TAATACGACTCACTATAGGAGTATTTCAGAAACACATGTTTTAGAGCTAGAAATAGC
nos2b sgRNA target-2	TAATACGACTCACTATAGGATGTGTTACATCACAGAGGTTTTAGAGCTAGAAATAGC
gsnor sgRNA target-1	TAATACGACTCACTATAGGCCCATGAAGTTCGAGTGAGTTTTAGAGCTAGAAATAGC
gsnor sgRNA target-2	TAATACGACTCACTATAGGTCATCCTGGGTCATGAGGGTTTTAGAGCTAGAAATAGC

Genotyping primers for gene disruption		
Gene symbol	**Primer forward**	**Primer reverse**
nos1-sgTarget-1	ATCGTCTCGGACCTCATCCG	ATAGGTTTTCTATTGCCCTGAGCTC
nos1-sgTarget-2	ATGCGAACGATGCTCGC	ATCCTTCCTATCGATGACCCTCTGG
nos2a-sgTarget-1	ATTACTGTTCTGTCGACTTGATAAACACG	ATACTTAAGATGAGTGCACAAGGCATG
nos2a-sgTarget-2	ATTTAGCCACTCTGAAATTCAAGCC	ATCAGTCCTTTGAAGCTGACCTTGC
nos2b-sgTarget-1	ATTGCAGCACGTTATACTCTCTTAGC	AATGGGCACTGCTTGACTTTAT
nos2b-sgTarget-2	ACTCACAAGAGCGAACTACTGC	ATTGACCCTTCACAAATCTTAGACG
gsnor-sgTarget-1	ATTAATTTTCAGGTGATCAAATGTAAGGC	ATGGGGTGAAGTTGAGTCAGC
gsnor-sgTarget-2	ATGTATTCAAAGTGTGTAATGTAGTCGG	TACCTGATTTTCTGGCACAGG

Supplementary Table S2. Plasmid construction primer sequences, related to STAR Methods.

Plasmid construction primer sequences			
Plasmid	**Elements**	**Primer forward**	**Primer reverse**
pTol2-cxcl18b: GFP	*cxcl18b-promoter*	TAGGGCGAATTGGGCATTTGTCTCCTCATGCATTGACTAC	AATTGCTGCAAACTATATGTAGGAAATGCTG
	GFP	ATGGTGAGCAAGGGC	TTACTTGTACAGCTCGTCCATGC
pTol2-cxcl18b: gal4FF	*gal4FF*	ATGAAGCTACTGTCTTCTATCGAACAAGC	CTACCCACCGTACTCGTCAATTCC
pTol2-cxcl18b: Cre-vmhc: mCherry	*Cre*	ATGGCCAATTTACTGACCGTACACC	CTAATCGCCATCTTCCAGCAGGC
	vmhc: mCherry	CATGTGTCCTAAATTCTGAAAACACAGTAAGCC	TTACTTGTACAGCTCGTCCATG
pTol2-UAS: Cas9-T2A-Cre-U6: nos2b sgRNA1; U6: nos2b sgRNA2	*nos2b sgRNA1*	CTCGGGTCGCTCTTGTGAGTGACC	AAACGGTCACTCACAAGAGCGACC
	nos2b sgRNA2	AGCTCGGGCTGGTGCCGCCAATGTCG	TAAACGACATTGGCGGCACCAGCCCG

Supplementary Table S3. qPCR primer sequences, related to STAR Methods.

Gene symbol	Primer forward	Primer reverse
cxcl18b	TGCTGCTCGCGGTAGTTTAC	TCTGCAGTAATTGGCCCTGC
glula	CGCATTACAGAGCCTGCCTA	ATTCCAGTTGCCTGGGATCG
glulb	ATGGTCCAGAACCAGCATCC	TCACAAGGGCCAACTTGGAA
pcna	CAGAAACCTAGCCATGGGGG	GTCTTGGACAGAGGAGTGGC
nos1	TGAGCACGTTTGCATAGGGT	CACTGGATTCGTCCCACACA
nos2a	CCAGATAACCACTGCTCTGCT	CTTGTCTTCCCATCTTGCTAAAA
nos2b	GAGGCAAAATTCCACCACCAG	TGCAAAGTGGTCATGGGACA
gsnor	ACAAGAAATCTCCACCCGGC	GACGGCTCGGATACTCTTCC
β-actin	ATTGCTGACAGGATGCAGAAG	GATGGTCCAGACTCATCGTACTC

Reference: Uncategorized References

Abalo, X.M., Lagman, D., Heras, G., Del Pozo, A., Eggert, J., and Larhammar, D. (2020). Circadian regulation of phosphodiesterase 6 genes in zebrafish differs between cones and rods: Implications for photopic and scotopic vision. Vision research *166*, 43-51.

Abraham, E., Hartmann, H., Yoshimatsu, T., Baden, T., and Brand, M. (2024). Restoration of cone-circuit functionality in the regenerating adult zebrafish retina. Developmental cell *59*, 2158-2170.e2156.

Asaoka, Y., Hata, S., Namae, M., Furutani-Seiki, M., and Nishina, H. (2014). The Hippo pathway controls a switch between retinal progenitor cell proliferation and photoreceptor cell differentiation in zebrafish. PloS one *9*, e97365.

Ashpole, N.M., Chawla, A.R., Martin, M.P., Brustovetsky, T., Brustovetsky, N., and Hudmon, A. (2013). Loss of calcium/calmodulin-dependent protein kinase II activity in cortical astrocytes decreases glutamate uptake and induces neurotoxic release of ATP. The Journal of biological chemistry *288*, 14599-14611.

Ashpole, N.M., Song, W., Brustovetsky, T., Engleman, E.A., Brustovetsky, N., Cummins, T.R., and Hudmon, A. (2012). Calcium/calmodulin-dependent protein kinase II (CaMKII) inhibition induces neurotoxicity via dysregulation of glutamate/calcium signaling and hyperexcitability. The Journal of biological chemistry *287*, 8495-8506.

Bedi, O., Sapra, V., Kumar, M., and Krishan, P. (2024). Newer mitochondrial dynamics and their role of calcium signalling in liver regeneration. Mitochondrion *79*, 101969.

Bernardos, R.L., and Raymond, P.A. (2006). GFAP transgenic zebrafish. Gene expression patterns : GEP *6*, 1007-1013.

1296 Boyd, P., Campbell, L.J., and Hyde, D.R. (2023). Clcf1/Crlf1a-mediated signaling is
1297 neuroprotective and required for Müller glia proliferation in the light-damaged zebrafish retina.
1298 Frontiers in cell and developmental biology *11*, 1142586.
1299 Bradley, S., Tossell, K., Lockley, R., and McDearmid, J.R. (2010). Nitric oxide synthase
1300 regulates morphogenesis of zebrafish spinal cord motoneurons. The Journal of neuroscience :
1301 the official journal of the Society for Neuroscience *30*, 16818-16831.
1302 Breus, O., and Dickmeis, T. (2021). Genetically encoded thiol redox-sensors in the zebrafish
1303 model: lessons for embryonic development and regeneration. Biological chemistry *402*, 363-
1304 378.
1305 Campbell, L.J., Hobgood, J.S., Jia, M., Boyd, P., Hipp, R.I., and Hyde, D.R. (2021). Notch3
1306 and DeltaB maintain Müller glia quiescence and act as negative regulators of regeneration in
1307 the light-damaged zebrafish retina. Glia *69*, 546-566.
1308 Campbell, L.J., Levendusky, J.L., Steines, S.A., and Hyde, D.R. (2022). Retinal regeneration
1309 requires dynamic Notch signaling. Neural regeneration research *17*, 1199-1209.
1310 Celotto, L., Rost, F., Machate, A., Bläsche, J., Dahl, A., Weber, A., Hans, S., and Brand, M.
1311 (2023). Single-cell RNA sequencing unravels the transcriptional network underlying zebrafish
1312 retina regeneration. eLife *12*.
1313 Charles, N., Ozawa, T., Squatrito, M., Bleau, A.M., Brennan, C.W., Hambardzumyan, D., and
1314 Holland, E.C. (2010). Perivascular nitric oxide activates notch signaling and promotes stem-
1315 like character in PDGF-induced glioma cells. Cell stem cell *6*, 141-152.
1316 Conner, C., Ackerman, K.M., Lahne, M., Hobgood, J.S., and Hyde, D.R. (2014). Repressing
1317 notch signaling and expressing TNFα are sufficient to mimic retinal regeneration by inducing

1318 Müller glial proliferation to generate committed progenitor cells. The Journal of neuroscience :
1319 the official journal of the Society for Neuroscience *34*, 14403-14419.
1320 Curado, S., Anderson, R.M., Jungblut, B., Mumm, J., Schroeter, E., and Stainier, D.Y. (2007).
1321 Conditional targeted cell ablation in zebrafish: a new tool for regeneration studies.
1322 Developmental dynamics : an official publication of the American Association of Anatomists
1323 *236*, 1025-1035.
1324 Curado, S., Stainier, D.Y., and Anderson, R.M. (2008). Nitroreductase-mediated cell/tissue
1325 ablation in zebrafish: a spatially and temporally controlled ablation method with applications in
1326 developmental and regeneration studies. Nature protocols *3*, 948-954.
1327 Dermietzel, R., Kremer, M., Paputsoglu, G., Stang, A., Skerrett, I.M., Gomes, D., Srinivas, M.,
1328 Janssen-Bienhold, U., Weiler, R., Nicholson, B.J.*, et al.* (2000). Molecular and functional
1329 diversity of neural connexins in the retina. The Journal of neuroscience : the official journal of
1330 the Society for Neuroscience *20*, 8331-8343.
1331 Di Donato, V., De Santis, F., Auer, T.O., Testa, N., Sánchez-Iranzo, H., Mercader, N.,
1332 Concordet, J.P., and Del Bene, F. (2016). 2C-Cas9: a versatile tool for clonal analysis of gene
1333 function. Genome research *26*, 681-692.
1334 Ellett, F., Pase, L., Hayman, J.W., Andrianopoulos, A., and Lieschke, G.J. (2011). mpeg1
1335 promoter transgenes direct macrophage-lineage expression in zebrafish. Blood *117*, e49-56.
1336 Fausett, B.V., Gumerson, J.D., and Goldman, D. (2008). The proneural basic helix-loop-helix
1337 gene ascl1a is required for retina regeneration. The Journal of neuroscience : the official
1338 journal of the Society for Neuroscience *28*, 1109-1117.
1339 Förstermann, U., and Sessa, W.C. (2012). Nitric oxide synthases: regulation and function.

1340 European heart journal *33*, 829-837, 837a-837d.

1341 Gao, H., A, L., Huang, X., Chen, X., and Xu, H. (2021). Müller Glia-Mediated Retinal

1342 Regeneration. Molecular neurobiology *58*, 2342-2361.

1343 Goldman, D. (2014). Müller glial cell reprogramming and retina regeneration. Nature reviews

1344 Neuroscience *15*, 431-442.

1345 Goldstein, S., Russo, A., and Samuni, A. (2003). Reactions of PTIO and carboxy-PTIO with

1346 *NO, *NO2, and O2-*. The Journal of biological chemistry *278*, 50949-50955.

1347 Gonzalez-Nunez, V., Nocco, V., and Budd, A. (2010). Characterization of drCol 15a1b: a

1348 novel component of the stem cell niche in the zebrafish retina. Stem cells (Dayton, Ohio) *28*,

1349 1399-1411.

1350 Gorsuch, R.A., Lahne, M., Yarka, C.E., Petravick, M.E., Li, J., and Hyde, D.R. (2017). Sox2

1351 regulates Müller glia reprogramming and proliferation in the regenerating zebrafish retina via

1352 Lin28 and Ascl1a. Experimental eye research *161*, 174-192.

1353 Goumenaki, P., Günther, S., Kikhi, K., Looso, M., Marín-Juez, R., and Stainier, D.Y.R. (2024).

1354 The innate immune regulator MyD88 dampens fibrosis during zebrafish heart regeneration.

1355 Nature cardiovascular research *3*, 1158-1176.

1356 Grover, L.M., and Teyler, T.J. (1990). Two components of long-term potentiation induced by

1357 different patterns of afferent activation. Nature *347*, 477-479.

1358 Han, P., Zhou, X.H., Chang, N., Xiao, C.L., Yan, S., Ren, H., Yang, X.Z., Zhang, M.L., Wu, Q.,

1359 Tang, B.*, et al.* (2014). Hydrogen peroxide primes heart regeneration with a derepression

1360 mechanism. Cell research *24*, 1091-1107.

1361 Hans, S., Kaslin, J., Freudenreich, D., and Brand, M. (2009). Temporally-controlled site-

1362 specific recombination in zebrafish. PloS one *4*, e4640.

1363 Hanson, Q.M., Carley, J.R., Gilbreath, T.J., Smith, B.C., and Underbakke, E.S. (2018).
1364 Calmodulin-induced Conformational Control and Allostery Underlying Neuronal Nitric Oxide
1365 Synthase Activation. Journal of molecular biology *430*, 935-947.

1366 Hoang, T., Wang, J., Boyd, P., Wang, F., Santiago, C., Jiang, L., Yoo, S., Lahne, M., Todd,
1367 L.J., Jia, M.*, et al.* (2020). Gene regulatory networks controlling vertebrate retinal regeneration.
1368 Science (New York, NY) *370*.

1369 Hong, J., Kim, B.K., Lim, H., Lee, S., and Lee, S.J. (2012). Identification and characterization
1370 of triamcinolone acetonide, a microglial-activation inhibitor. Immunopharmacology and
1371 immunotoxicology *34*, 912-918.

1372 Hunter, M.V., Willoughby, P.M., Bruce, A.E.E., and Fernandez-Gonzalez, R. (2018). Oxidative
1373 Stress Orchestrates Cell Polarity to Promote Embryonic Wound Healing. Developmental cell
1374 *47*, 377-387.e374.

1375 Iribarne, M., and Hyde, D.R. (2022). Different inflammation responses modulate Müller glia
1376 proliferation in the acute or chronically damaged zebrafish retina. Frontiers in cell and
1377 developmental biology *10*, 892271.

1378 Jaeschke, H. (2000). Reactive oxygen and mechanisms of inflammatory liver injury. Journal
1379 of gastroenterology and hepatology *15*, 718-724.

1380 Janssen-Bienhold, U., Dermietzel, R., and Weiler, R. (1998). Distribution of connexin43
1381 immunoreactivity in the retinas of different vertebrates. The Journal of comparative neurology
1382 *396*, 310-321.

1383 Jia, W., Channappanavar, R., Zhang, C., Li, M., Zhou, H., Zhang, S., Zhou, P., Xu, J., Shan,

1384 S., Shi, X., *et al.* (2019). Single intranasal immunization with chimpanzee adenovirus-based
1385 vaccine induces sustained and protective immunity against MERS-CoV infection. Emerging
1386 microbes & infections *8*, 760-772.
1387 Jones, R.J., Jourd'heuil, D., Salerno, J.C., Smith, S.M., and Singer, H.A. (2007). iNOS
1388 regulation by calcium/calmodulin-dependent protein kinase II in vascular smooth muscle.
1389 American journal of physiology Heart and circulatory physiology *292*, H2634-2642.
1390 Jorstad, N.L., Wilken, M.S., Grimes, W.N., Wohl, S.G., VandenBosch, L.S., Yoshimatsu, T.,
1391 Wong, R.O., Rieke, F., and Reh, T.A. (2017). Stimulation of functional neuronal regeneration
1392 from Müller glia in adult mice. Nature *548*, 103-107.
1393 Kawamoto, E.M., Vivar, C., and Camandola, S. (2012). Physiology and pathology of calcium
1394 signaling in the brain. Frontiers in pharmacology *3*, 61.
1395 Kimura, M., Moteki, H., and Ogihara, M. (2023). Role of Hepatocyte Growth Regulators in
1396 Liver Regeneration. Cells *12*.
1397 Krylov, A., Yu, S., Veen, K., Newton, A., Ye, A., Qin, H., He, J., and Jusuf, P.R. (2023).
1398 Heterogeneity in quiescent Müller glia in the uninjured zebrafish retina drive differential
1399 responses following photoreceptor ablation. Frontiers in molecular neuroscience *16*, 1087136.
1400 Kwan, K.M., Fujimoto, E., Grabher, C., Mangum, B.D., Hardy, M.E., Campbell, D.S., Parant,
1401 J.M., Yost, H.J., Kanki, J.P., and Chien, C.B. (2007). The Tol2kit: a multisite gateway-based
1402 construction kit for Tol2 transposon transgenesis constructs. Developmental dynamics : an
1403 official publication of the American Association of Anatomists *236*, 3088-3099.
1404 Kyritsis, N., Kizil, C., Zocher, S., Kroehne, V., Kaslin, J., Freudenreich, D., Iltzsche, A., and
1405 Brand, M. (2012). Acute inflammation initiates the regenerative response in the adult

1406 zebrafish brain. Science (New York, NY) *338*, 1353-1356.

1407 Lahne, M., Brecker, M., Jones, S.E., and Hyde, D.R. (2020a). The Regenerating Adult

1408 Zebrafish Retina Recapitulates Developmental Fate Specification Programs. Frontiers in cell

1409 and developmental biology *8*, 617923.

1410 Lahne, M., Nagashima, M., Hyde, D.R., and Hitchcock, P.F. (2020b). Reprogramming Müller

1411 Glia to Regenerate Retinal Neurons. Annual review of vision science *6*, 171-193.

1412 Leach, L.L., Hanovice, N.J., George, S.M., Gabriel, A.E., and Gross, J.M. (2021). The

1413 immune response is a critical regulator of zebrafish retinal pigment epithelium regeneration.

1414 Proceedings of the National Academy of Sciences of the United States of America *118*.

1415 Lee, M.S., Jui, J., Sahu, A., and Goldman, D. (2024). Mycb and Mych stimulate Müller glial

1416 cell reprogramming and proliferation in the uninjured and injured zebrafish retina.

1417 Development (Cambridge, England) *151*.

1418 Lee, M.S., Wan, J., and Goldman, D. (2020). Tgfb3 collaborates with PP2A and notch

1419 signaling pathways to inhibit retina regeneration. eLife *9*.

1420 Lenkowski, J.R., and Raymond, P.A. (2014). Müller glia: Stem cells for generation and

1421 regeneration of retinal neurons in teleost fish. Progress in retinal and eye research *40*, 94-123.

1422 Levin, M. (2009). Bioelectric mechanisms in regeneration: Unique aspects and future

1423 perspectives. Seminars in cell & developmental biology *20*, 543-556.

1424 Liu, J., Xu, K., Xing, M., Zhuo, Y., Guo, J., Du, M., Wang, Q., An, Y., Li, J., Gao, P.*, et al.*

1425 (2021). Heterologous prime-boost immunizations with chimpanzee adenoviral vectors elicit

1426 potent and protective immunity against SARS-CoV-2 infection. Cell discovery *7*, 123.

1427 López-Juárez, A., Titus, H.E., Silbak, S.H., Pressler, J.W., Rizvi, T.A., Bogard, M., Bennett,

1428 M.R., Ciraolo, G., Williams, M.T., Vorhees, C.V., *et al.* (2017). Oligodendrocyte Nf1 Controls
1429 Aberrant Notch Activation and Regulates Myelin Structure and Behavior. Cell reports *19*, 545-
1430 557.
1431 Lu, C., and Hyde, D.R. (2024). Cytokines IL-1β and IL-10 are required for Müller glia
1432 proliferation following light damage in the adult zebrafish retina. Frontiers in cell and
1433 developmental biology *12*, 1406330.
1434 Lyu, P., Iribarne, M., Serjanov, D., Zhai, Y., Hoang, T., Campbell, L.J., Boyd, P., Palazzo, I.,
1435 Nagashima, M., Silva, N.J., *et al.* (2023). Common and divergent gene regulatory networks
1436 control injury-induced and developmental neurogenesis in zebrafish retina. Nat Commun *14*,
1437 8477.
1438 Matrone, G., Jung, S.Y., Choi, J.M., Jain, A., Leung, H.E., Rajapakshe, K., Coarfa, C., Rodor,
1439 J., Denvir, M.A., Baker, A.H., *et al.* (2021). Nuclear S-nitrosylation impacts tissue regeneration
1440 in zebrafish. Nat Commun *12*, 6282.
1441 Meng, J., Lv, Z., Zhang, Y., Wang, Y., Qiao, X., Sun, C., Chen, Y., Guo, M., Han, W., Ye, A.,
1442 *et al.* (2021). Precision Redox: The Key for Antioxidant Pharmacology. Antioxidants & redox
1443 signaling *34*, 1069-1082.
1444 Moore, P.K., al-Swayeh, O.A., Chong, N.W., Evans, R.A., and Gibson, A. (1990). L-NG-nitro
1445 arginine (L-NOARG), a novel, L-arginine-reversible inhibitor of endothelium-dependent
1446 vasodilatation in vitro. British journal of pharmacology *99*, 408-412.
1447 Nelson, C.M., Ackerman, K.M., O'Hayer, P., Bailey, T.J., Gorsuch, R.A., and Hyde, D.R.
1448 (2013). Tumor necrosis factor-alpha is produced by dying retinal neurons and is required for
1449 Muller glia proliferation during zebrafish retinal regeneration. The Journal of neuroscience :

1450 the official journal of the Society for Neuroscience *33*, 6524-6539.

1451 Pacher, P., Beckman, J.S., and Liaudet, L. (2007). Nitric oxide and peroxynitrite in health and

1452 disease. Physiological reviews *87*, 315-424.

1453 Park, M. (2018). AMPA Receptor Trafficking for Postsynaptic Potentiation. Frontiers in cellular

1454 neuroscience *12*, 361.

1455 Parsons, M.J., Pisharath, H., Yusuff, S., Moore, J.C., Siekmann, A.F., Lawson, N., and Leach,

1456 S.D. (2009). Notch-responsive cells initiate the secondary transition in larval zebrafish

1457 pancreas. Mechanisms of development *126*, 898-912.

1458 Picelli, S., Björklund Å, K., Faridani, O.R., Sagasser, S., Winberg, G., and Sandberg, R.

1459 (2013). Smart-seq2 for sensitive full-length transcriptome profiling in single cells. Nature

1460 methods *10*, 1096-1098.

1461 Pollak, J., Wilken, M.S., Ueki, Y., Cox, K.E., Sullivan, J.M., Taylor, R.J., Levine, E.M., and

1462 Reh, T.A. (2013). ASCL1 reprograms mouse Muller glia into neurogenic retinal progenitors.

1463 Development (Cambridge, England) *140*, 2619-2631.

1464 Powell, C., Cornblath, E., Elsaeidi, F., Wan, J., and Goldman, D. (2016). Zebrafish Müller glia-

1465 derived progenitors are multipotent, exhibit proliferative biases and regenerate excess

1466 neurons. Scientific reports *6*, 24851.

1467 Qin, C., Qi, Z., Pan, S., Xia, P., Kong, W., Sun, B., Du, H., Zhang, R., Zhu, L., Zhou, D.*, et al.*

1468 (2023). Advances in Conductive Hydrogel for Spinal Cord Injury Repair and Regeneration.

1469 International journal of nanomedicine *18*, 7305-7333.

1470 Quillien, A., Moore, J.C., Shin, M., Siekmann, A.F., Smith, T., Pan, L., Moens, C.B., Parsons,

1471 M.J., and Lawson, N.D. (2014). Distinct Notch signaling outputs pattern the developing

1472 arterial system. Development (Cambridge, England) *141*, 1544-1552.

1473 Ramachandran, R., Fausett, B.V., and Goldman, D. (2010). Ascl1a regulates Müller glia

1474 dedifferentiation and retinal regeneration through a Lin-28-dependent, let-7 microRNA

1475 signalling pathway. Nature cell biology *12*, 1101-1107.

1476 Raymond, P.A., Barthel, L.K., Bernardos, R.L., and Perkowski, J.J. (2006). Molecular

1477 characterization of retinal stem cells and their niches in adult zebrafish. BMC developmental

1478 biology *6*, 36.

1479 Rees, D.D., Palmer, R.M., Schulz, R., Hodson, H.F., and Moncada, S. (1990).

1480 Characterization of three inhibitors of endothelial nitric oxide synthase in vitro and in vivo.

1481 British journal of pharmacology *101*, 746-752.

1482 Rochon, E.R., Missinato, M.A., Xue, J., Tejero, J., Tsang, M., Gladwin, M.T., and Corti, P.

1483 (2020). Nitrite Improves Heart Regeneration in Zebrafish. Antioxidants & redox signaling *32*,

1484 363-377.

1485 Sahu, A., Devi, S., Jui, J., and Goldman, D. (2021). Notch signaling via Hey1 and Id2b

1486 regulates Müller glia's regenerative response to retinal injury. Glia *69*, 2882-2898.

1487 Shen, Y.C., and Raymond, P.A. (2004). Zebrafish cone-rod (crx) homeobox gene promotes

1488 retinogenesis. Developmental biology *269*, 237-251.

1489 Sifuentes, C.J., Kim, J.W., Swaroop, A., and Raymond, P.A. (2016). Rapid, Dynamic

1490 Activation of Müller Glial Stem Cell Responses in Zebrafish. Investigative ophthalmology &

1491 visual science *57*, 5148-5160.

1492 Silva, N.J., Nagashima, M., Li, J., Kakuk-Atkins, L., Ashrafzadeh, M., Hyde, D.R., and

1493 Hitchcock, P.F. (2020). Inflammation and matrix metalloproteinase 9 (Mmp-9) regulate

1494 photoreceptor regeneration in adult zebrafish. Glia *68*, 1445-1465.

1495 Tang, X., Gao, J., Jia, X., Zhao, W., Zhang, Y., Pan, W., and He, J. (2017). Bipotent

1496 progenitors as embryonic origin of retinal stem cells. The Journal of cell biology *216*, 1833-

1497 1847.

1498 Thummel, R., Kassen, S.C., Enright, J.M., Nelson, C.M., Montgomery, J.E., and Hyde, D.R.

1499 (2008). Characterization of Müller glia and neuronal progenitors during adult zebrafish retinal

1500 regeneration. Experimental eye research *87*, 433-444.

1501 Torraca, V., Otto, N.A., Tavakoli-Tameh, A., and Meijer, A.H. (2017). The inflammatory

1502 chemokine Cxcl18b exerts neutrophil-specific chemotaxis via the promiscuous chemokine

1503 receptor Cxcr2 in zebrafish. Developmental and comparative immunology *67*, 57-65.

1504 Vihtelic, T.S., and Hyde, D.R. (2000). Light-induced rod and cone cell death and regeneration

1505 in the adult albino zebrafish (Danio rerio) retina. Journal of neurobiology *44*, 289-307.

1506 Villegas, S.N., Gombos, R., García-López, L., Gutiérrez-Pérez, I., García-Castillo, J., Vallejo,

1507 D.M., Da Ros, V.G., Ballesta-Illán, E., Mihály, J., and Dominguez, M. (2018). PI3K/Akt

1508 Cooperates with Oncogenic Notch by Inducing Nitric Oxide-Dependent Inflammation. Cell

1509 reports *22*, 2541-2549.

1510 Wan, J., and Goldman, D. (2016). Retina regeneration in zebrafish. Current opinion in

1511 genetics & development *40*, 41-47.

1512 Wan, J., and Goldman, D. (2017). Opposing Actions of Fgf8a on Notch Signaling Distinguish

1513 Two Muller Glial Cell Populations that Contribute to Retina Growth and Regeneration. Cell

1514 reports *19*, 849-862.

1515 Wan, J., Ramachandran, R., and Goldman, D. (2012). HB-EGF is necessary and sufficient for

1516 Müller glia dedifferentiation and retina regeneration. Developmental cell *22*, 334-347.

1517 Wang, H., Yang, Z., Li, X., Huang, D., Yu, S., He, J., Li, Y., and Yan, J. (2020). Single-cell in

1518 vivo imaging of cellular circadian oscillators in zebrafish. PLoS biology *18*, e3000435.

1519 White, D.T., Sengupta, S., Saxena, M.T., Xu, Q., Hanes, J., Ding, D., Ji, H., and Mumm, J.S.

1520 (2017). Immunomodulation-accelerated neuronal regeneration following selective rod

1521 photoreceptor cell ablation in the zebrafish retina. Proceedings of the National Academy of

1522 Sciences of the United States of America *114*, E3719-e3728.

1523 Wu, D.M., Schneiderman, T., Burgett, J., Gokhale, P., Barthel, L., and Raymond, P.A. (2001).

1524 Cones regenerate from retinal stem cells sequestered in the inner nuclear layer of adult

1525 goldfish retina. Investigative ophthalmology & visual science *42*, 2115-2124.

1526 Wu, K., Ren, R., Su, W., Wen, B., Zhang, Y., Yi, F., Qiao, X., Yuan, T., Wang, J., Liu, L.*, et al.*

1527 (2014). A novel suppressive effect of alcohol dehydrogenase 5 in neuronal differentiation. The

1528 Journal of biological chemistry *289*, 20193-20199.

1529 Wu, R.S., Lam, II, Clay, H., Duong, D.N., Deo, R.C., and Coughlin, S.R. (2018). A Rapid

1530 Method for Directed Gene Knockout for Screening in G0 Zebrafish. Developmental cell *46*,

1531 112-125.e114.

1532 Xiao, X., Liao, Z., and Zou, J. (2023). Genetic and epigenetic regulators of retinal Müller glial

1533 cell reprogramming. Advances in ophthalmology practice and research *3*, 126-133.

1534 Xu, B., Tang, X., Jin, M., Zhang, H., Du, L., Yu, S., and He, J. (2020). Unifying developmental

1535 programs for embryonic and postembryonic neurogenesis in the zebrafish retina.

1536 Development (Cambridge, England) *147*.

1537 Yao, K., Qiu, S., Tian, L., Snider, W.D., Flannery, J.G., Schaffer, D.V., and Chen, B. (2016).

1538 Wnt Regulates Proliferation and Neurogenic Potential of Müller Glial Cells via a Lin28/let-7
1539 miRNA-Dependent Pathway in Adult Mammalian Retinas. Cell reports *17*, 165-178.
1540 Yeo, S.Y., Kim, M., Kim, H.S., Huh, T.L., and Chitnis, A.B. (2007). Fluorescent protein
1541 expression driven by her4 regulatory elements reveals the spatiotemporal pattern of Notch
1542 signaling in the nervous system of zebrafish embryos. Developmental biology *301*, 555-567.
1543 Yoo, S.K., Freisinger, C.M., LeBert, D.C., and Huttenlocher, A. (2012). Early redox, Src family
1544 kinase, and calcium signaling integrate wound responses and tissue regeneration in zebrafish.
1545 The Journal of cell biology *199*, 225-234.
1546 Yu, C., Li, X., Ma, J., Liang, S., Zhao, Y., Li, Q., and Zhang, R. (2024). Spatiotemporal
1547 modulation of nitric oxide and Notch signaling by hemodynamic-responsive Trpv4 is essential
1548 for ventricle regeneration. Cellular and molecular life sciences : CMLS *81*, 60.
1549 Yu, S., and He, J. (2019). Stochastic cell-cycle entry and cell-state-dependent fate outputs of
1550 injury-reactivated tectal radial glia in zebrafish. eLife *8*.
1551 Yurco, P., and Cameron, D.A. (2005). Responses of Müller glia to retinal injury in adult
1552 zebrafish. Vision research *45*, 991-1002.
1553 Zhang, H., Hao, J., Hong, H., Gu, W., Li, Z., Sun, J., Zhan, H., Wei, X., and Zhou, L. (2024).
1554 Redox signaling regulates the skeletal tissue development and regeneration. Biotechnology &
1555 genetic engineering reviews *40*, 2308-2331.
1556 Zhang, Z., Hou, H., Yu, S., Zhou, C., Zhang, X., Li, N., Zhang, S., Song, K., Lu, Y., Liu, D.*, et*
1557 *al.* (2020). Inflammation-induced mammalian target of rapamycin signaling is essential for
1558 retina regeneration. Glia *68*, 111-127.
1559

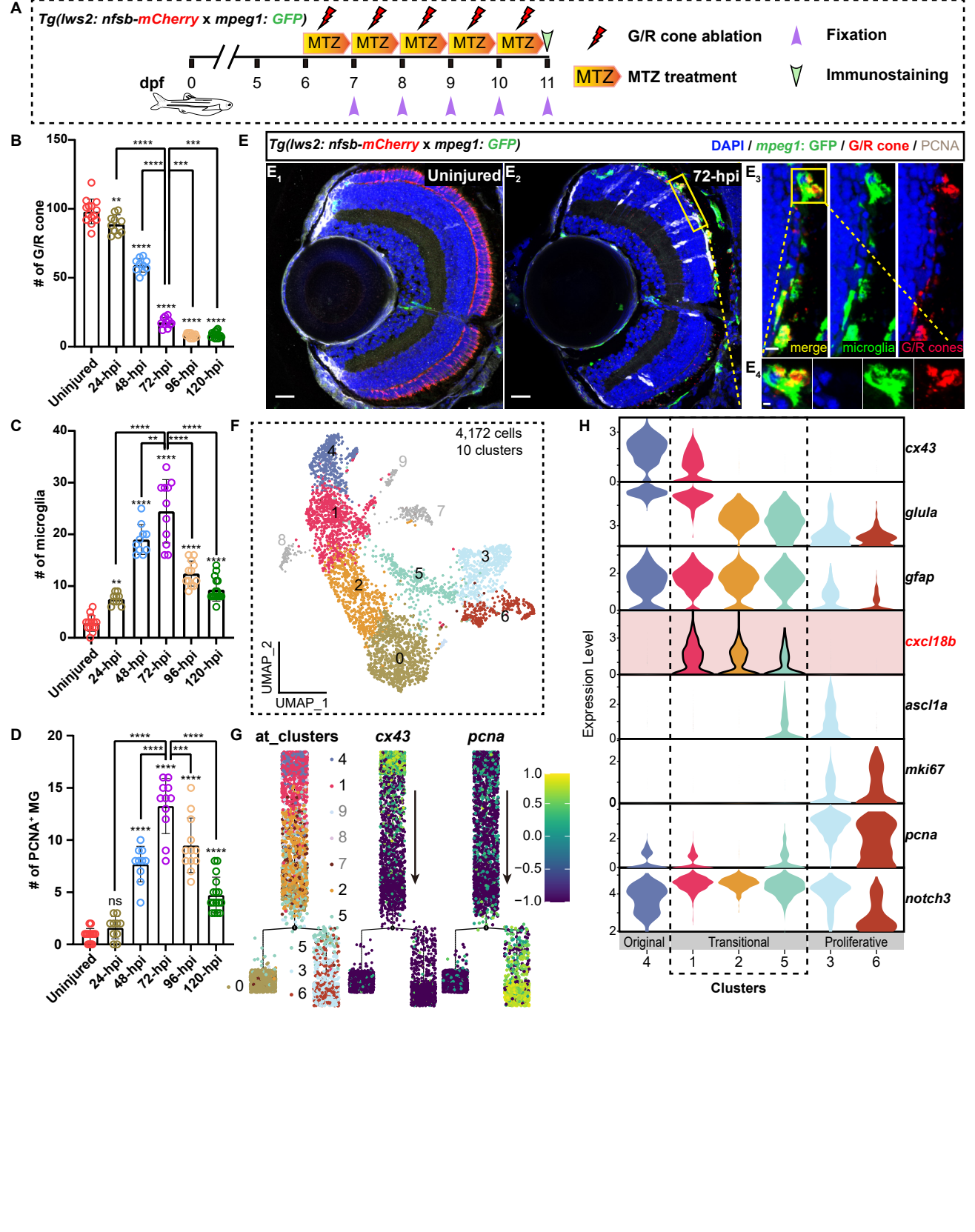
A
Tg(lws2: nfsb-mCherry x mpeg1: GFP)
MTZ
dpf
0
5
6
7
8
9
10
11
G/R cone ablation
MTZ treatment
Fixation
Immunostaining
B
# of G/R cone
Uninjured
24-hpi
48-hpi
72-hpi
96-hpi
120-hpi
E
Tg(lws2: nfsb-mCherry x mpeg1: GFP)
DAPI / mpeg1: GFP / G/R cone / PCNA
Uninjured
72-hpi
merge
microglia
G/R cones
C
# of microglia
F
4,172 cells
10 clusters
UMAP_2
UMAP_1
H
cx43
glula
gfap
cxcl18b
ascl1a
mki67
pcna
notch3
Expression Level
Original
Transitional
Proliferative
Clusters
D
# of PCNA+ MG
ns
G
at_clusters
cx43
pcna

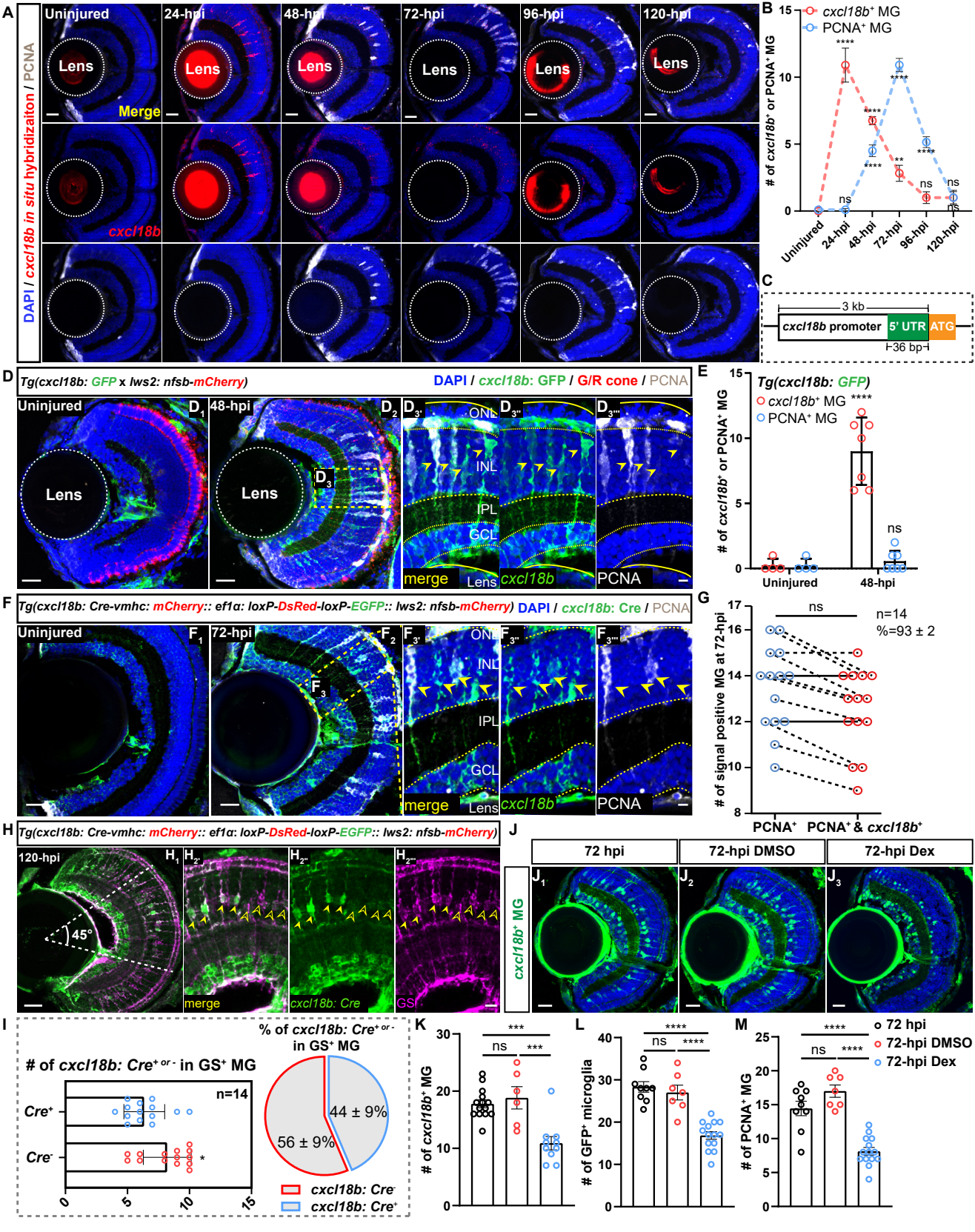
A
DAPI / cxcl18b in situ hybridizaiton / PCNA
Uninjured
24-hpi
48-hpi
72-hpi
96-hpi
120-hpi
Lens
Merge
cxcl18b
B
cxcl18b+ MG
PCNA+ MG
# of cxcl18b+ or PCNA+ MG
Uninjured
24-hpi
48-hpi
72-hpi
96-hpi
120-hpi
C
3 kb
cxcl18b promoter
5' UTR
ATG
36 bp
D
Tg(cxcl18b: GFP x lws2: nfsb-mCherry)
DAPI / cxcl18b: GFP / G/R cone / PCNA
Uninjured
48-hpi
Lens
ONL
INL
IPL
GCL
merge
cxcl18b
PCNA
E
Tg(cxcl18b: GFP)
cxcl18b+ MG
PCNA+ MG
# of cxcl18b+ or PCNA+ MG
Uninjured
48-hpi
ns
F
Tg(cxcl18b: Cre-vmhc: mCherry:: ef1α: loxP-DsRed-loxP-EGFP:: lws2: nfsb-mCherry)
DAPI / cxcl18b: Cre / PCNA
Uninjured
72-hpi
ONL
INL
IPL
GCL
merge
cxcl18b
PCNA
G
ns
n=14
%=93 ± 2
# of signal positive MG at 72-hpi
PCNA+
PCNA+ & cxcl18b+
H
Tg(cxcl18b: Cre-vmhc: mCherry:: ef1α: loxP-DsRed-loxP-EGFP:: lws2: nfsb-mCherry)
120-hpi
45°
merge
cxcl18b: Cre
GS
J
72 hpi
72-hpi DMSO
72-hpi Dex
cxcl18b+ MG
I
# of cxcl18b: Cre+ or - in GS+ MG
n=14
Cre+
Cre-
% of cxcl18b: Cre+ or - in GS+ MG
44 ± 9%
56 ± 9%
cxcl18b: Cre-
cxcl18b: Cre+
K
# of cxcl18b+ MG
ns
L
# of GFP+ microglia
ns
M
# of PCNA+ MG
ns
72 hpi
72-hpi DMSO
72-hpi Dex

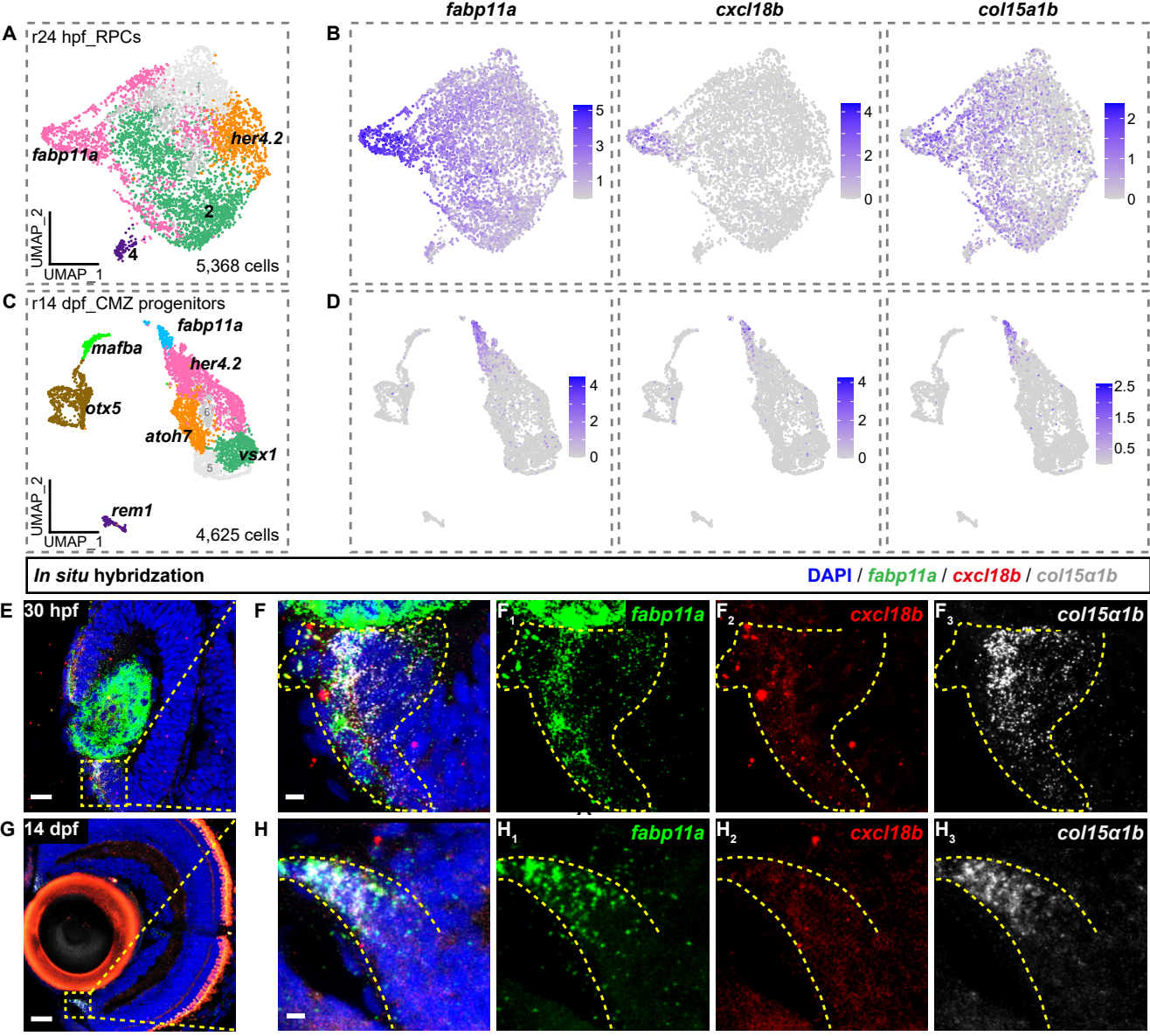
fabp11a
cxcl18b
col15a1b
A
r24 hpf_RPCs
fabp11a
her4.2
2
4
UMAP_2
UMAP_1
5,368 cells
B
C
r14 dpf_CMZ progenitors
fabp11a
mafba
her4.2
otx5
atoh7
vsx1
rem1
4,625 cells
D
In situ hybridzation
DAPI / fabp11a / cxcl18b / col15a1b
E
30 hpf
F
F1
fabp11a
F2
cxcl18b
F3
col15a1b
G
14 dpf
H
H1
fabp11a
H2
cxcl18b
H3
col15a1b

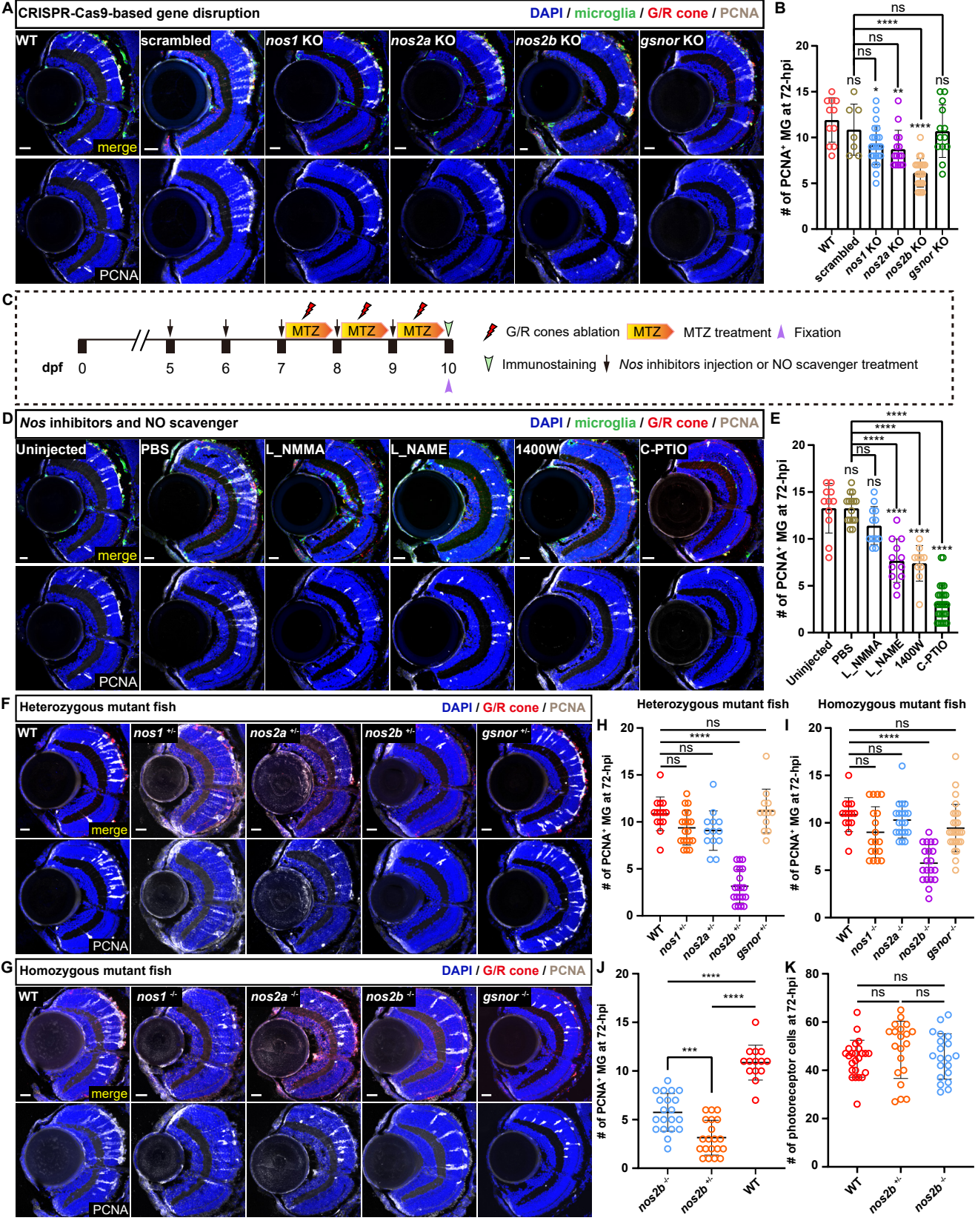
A
CRISPR-Cas9-based gene disruption
DAPI / microglia / G/R cone / PCNA
WT
scrambled
nos1 KO
nos2a KO
nos2b KO
gsnor KO
merge
PCNA
B
# of PCNA+ MG at 72-hpi
ns
****
*
**
C
dpf
0
5
6
7
8
9
10
MTZ
G/R cones ablation
MTZ treatment
Fixation
Immunostaining
Nos inhibitors injection or NO scavenger treatment
D
Nos inhibitors and NO scavenger
Uninjected
PBS
L_NMMA
L_NAME
1400W
C-PTIO
E
F
Heterozygous mutant fish
nos1 +/-
nos2a +/-
nos2b +/-
gsnor +/-
G
Homozygous mutant fish
nos1 -/-
nos2a -/-
nos2b -/-
gsnor -/-
H
I
J
K
# of photoreceptor cells at 72-hpi
***

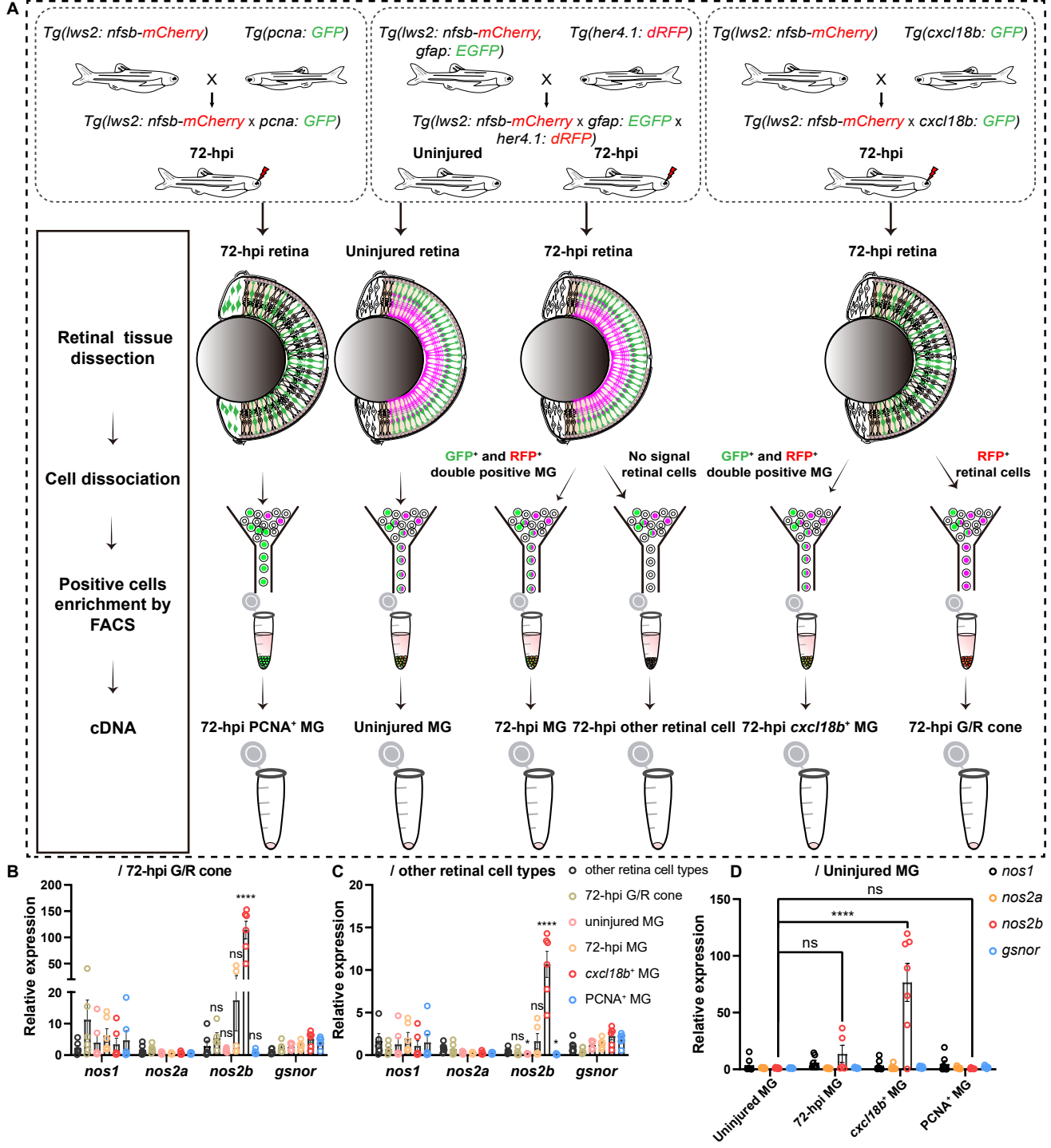
A
Tg(lws2: nfsb-mCherry)
Tg(pcna: GFP)
Tg(lws2: nfsb-mCherry x pcna: GFP)
72-hpi
Tg(lws2: nfsb-mCherry, gfap: EGFP)
Tg(her4.1: dRFP)
Tg(lws2: nfsb-mCherry x gfap: EGFP x her4.1: dRFP)
Uninjured
72-hpi
Tg(lws2: nfsb-mCherry)
Tg(cxcl18b: GFP)
Tg(lws2: nfsb-mCherry x cxcl18b: GFP)
72-hpi
Retinal tissue dissection
Cell dissociation
Positive cells enrichment by FACS
cDNA
72-hpi retina
Uninjured retina
72-hpi retina
72-hpi retina
GFP+ and RFP+ double positive MG
No signal retinal cells
GFP+ and RFP+ double positive MG
RFP+ retinal cells
72-hpi PCNA+ MG
Uninjured MG
72-hpi MG
72-hpi other retinal cell
72-hpi cxcl18b+ MG
72-hpi G/R cone
B
/ 72-hpi G/R cone
Relative expression
nos1
nos2a
nos2b
gsnor
C
/ other retinal cell types
other retina cell types
72-hpi G/R cone
uninjured MG
72-hpi MG
cxcl18b+ MG
PCNA+ MG
D
/ Uninjured MG
nos1
nos2a
nos2b
gsnor
Uninjured MG
72-hpi MG
cxcl18b+ MG
PCNA+ MG

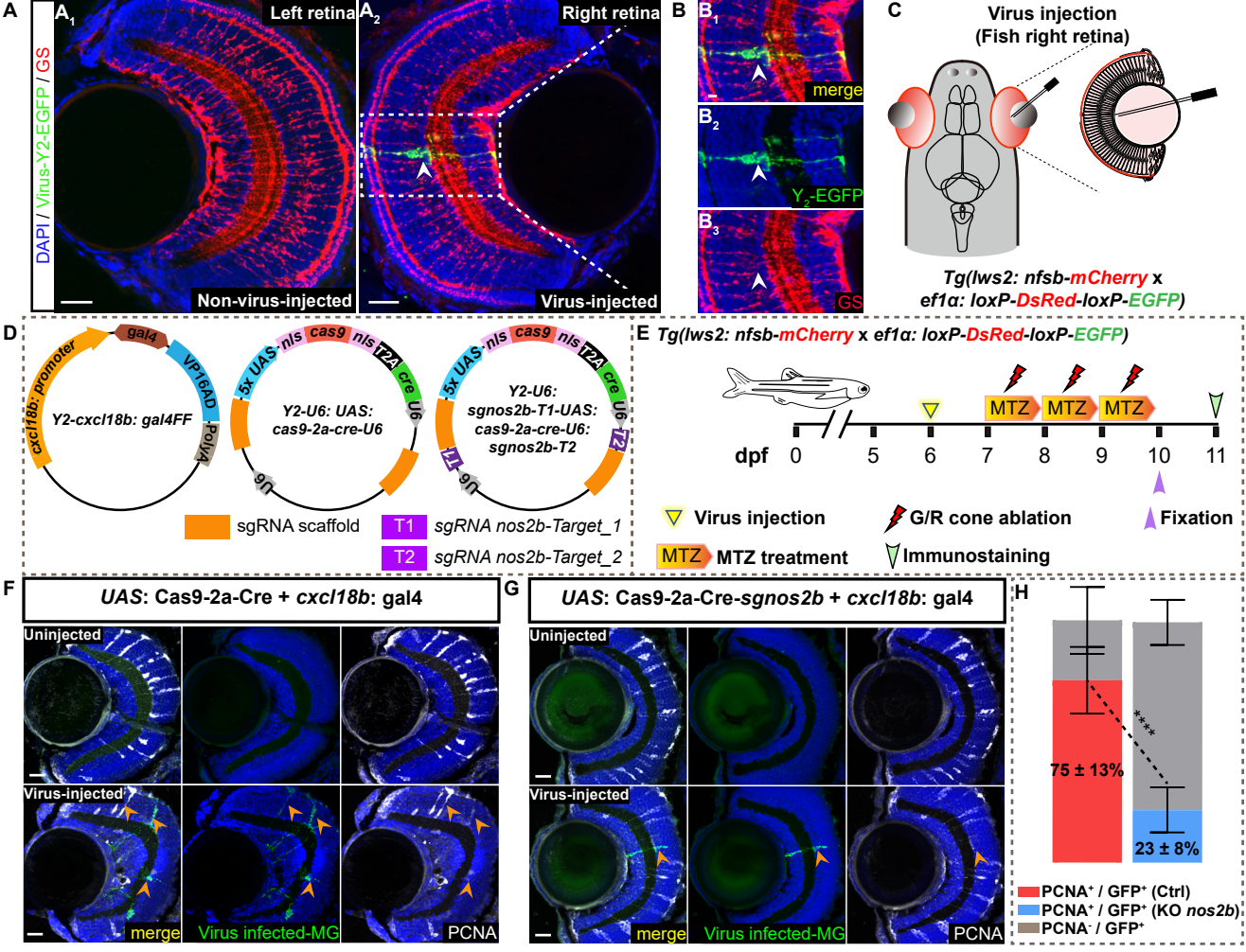
A
A1
Left retina
A2
Right retina
DAPI / Virus-Y2-EGFP / GS
Non-virus-injected
Virus-injected
B
B1
merge
B2
Y2-EGFP
B3
GS
C
Virus injection
(Fish right retina)
Tg(lws2: nfsb-mCherry x
ef1α: loxP-DsRed-loxP-EGFP)
D
gal4
VP16AD
PolyA
cxcl18b: promoter
Y2-cxcl18b: gal4FF
5x UAS
nls
cas9
nls
T2A
cre
U6
Y2-U6: UAS:
cas9-2a-cre-U6
Y2-U6:
sgnos2b-T1-UAS:
cas9-2a-cre-U6:
sgnos2b-T2
T1
T2
sgRNA scaffold
T1 sgRNA nos2b-Target_1
T2 sgRNA nos2b-Target_2
E Tg(lws2: nfsb-mCherry x ef1α: loxP-DsRed-loxP-EGFP)
MTZ
dpf 0 5 6 7 8 9 10 11
Virus injection
G/R cone ablation
Fixation
MTZ treatment
Immunostaining
F
UAS: Cas9-2a-Cre + cxcl18b: gal4
Uninjected
Virus-injected
merge
Virus infected-MG
PCNA
G
UAS: Cas9-2a-Cre-sgnos2b + cxcl18b: gal4
Uninjected
Virus-injected
merge
Virus infected-MG
PCNA
H
75 ± 13%
23 ± 8%
***
PCNA+ / GFP+ (Ctrl)
PCNA+ / GFP+ (KO nos2b)
PCNA- / GFP+

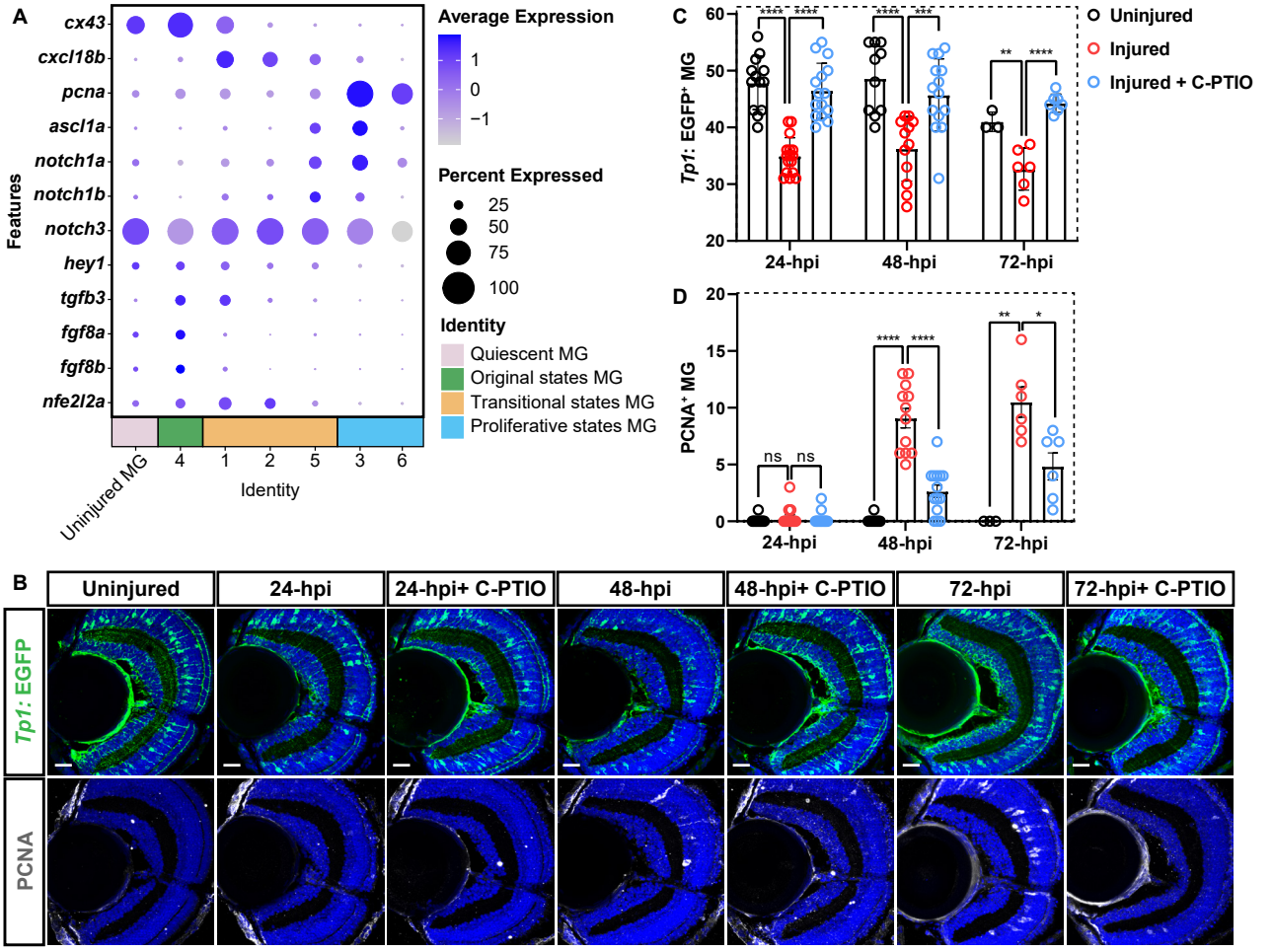
A
Features
cx43
cxcl18b
pcna
ascl1a
notch1a
notch1b
notch3
hey1
tgfb3
fgf8a
fgf8b
nfe2l2a
Uninjured MG
4
1
2
5
3
6
Identity
Average Expression
1
0
−1
Percent Expressed
25
50
75
100
Identity
Quiescent MG
Original states MG
Transitional states MG
Proliferative states MG
C
Tp1: EGFP+ MG
24-hpi
48-hpi
72-hpi
Uninjured
Injured
Injured + C-PTIO
D
PCNA+ MG
ns
B
Uninjured
24-hpi
24-hpi+ C-PTIO
48-hpi
48-hpi+ C-PTIO
72-hpi
72-hpi+ C-PTIO
Tp1: EGFP
PCNA